

Martin O'Mullane

**ITER2: ITER visits and support activities
Report 2**

10 Feb 2014

Workpackages : 2-3 and 3-4

Category : DRAFT – CONFIDENTIAL

This document has been prepared as part of the ADAS-EU Project. It is subject to change without notice. Please contact the authors before referencing it in peer-reviewed literature.
© Copyright, The ADAS Project.

ITER2: ITER visits and support activities Report 2

Martin O'Mullane

Department of Physics, University of Strathclyde, Glasgow, UK

Abstract: *Visits and support actions, on-site and off-site, provided under ADAS-EU to the ITER Organization in the reporting period: months YY-ZZ.*

Contents

1	Overview	2
2	Core X-ray Imaging spectrometer	3
3	Bolometer	6
4	Divertor Impurity Monitor	10
5	Working visits to ITER	47

Chapter 1

Overview

An important goal of the Support Action was to strengthen the atomic physics base required for ITER. The working relations, fostered by ADAS-EU, was considered to be successful and from October 2011 ITER is now directly funding this activity thus freeing up resources for other ADAS-EU activities.

The principal activity is the forward modelling of expected emission to aid spectroscopic design. Three systems were considered in this reporting period — the core X-ray imaging spectrometer, the bolometer and the divertor impurity monitoring system. This report details the emission model inputs to the design reviews of these instruments.

Chapter 2

Core X-ray Imaging spectrometer

This primary role of this instrument is to measure the confined plasma ion temperature and plasma rotation, both toroidal and poloidal. An accuracy of 10% is expected for a spatial resolution of $0.03a$, where a is the minor radius. Rotation is required to be measured to a time resolution of 0.01s with a reduced resolution requirement of 0.1s for temperature. A radial coverage of $0 < \rho < 0.85a$, (ideally $0.9a$) implies plasma conditions ranging from 4keV to the ITER goal of 25keV, and possibly higher. Other complementary systems are dedicated to general impurity survey spectroscopy and to localized coverage of the pedestal, edge and SOL plasma.

The instrument will consist of 3 crystal spectrometers mounted in an equatorial port plug to maximize spatial coverage. Figure 2.1 shows the adopted arrangement.

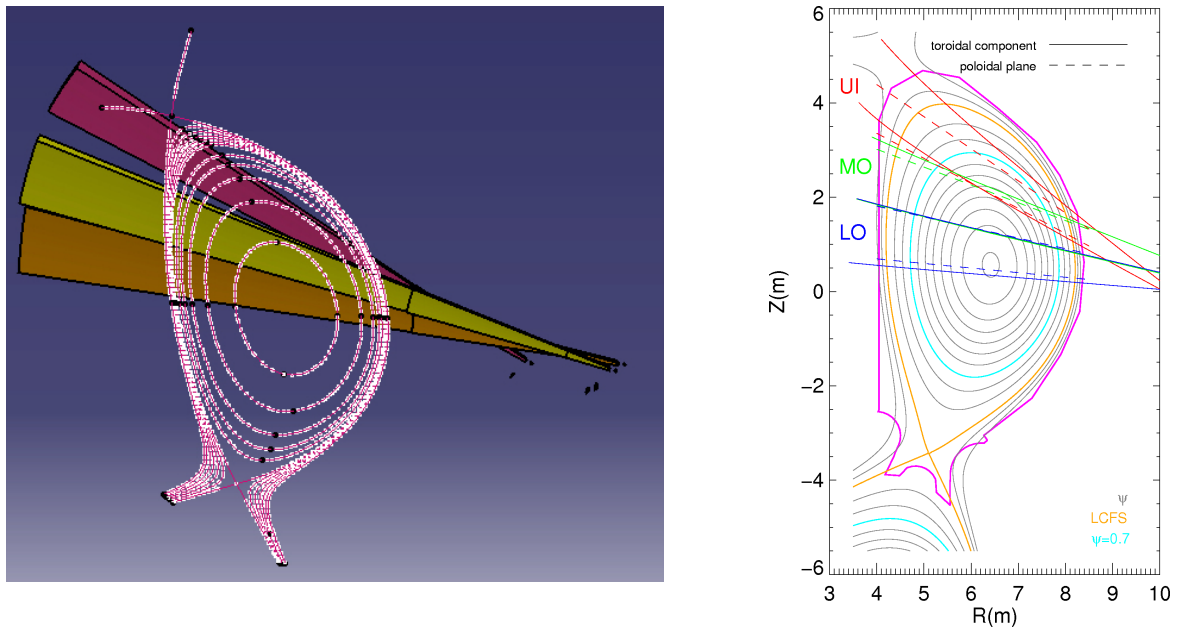


Figure 2.1: (left) CAD model of the 3 spectrometer lines of sight. (right) The LOS mapped onto the poloidal plane.

A toroidal component in the line of sight extends outwards the accessible plasma region. This complicates the poloidal rotation measurement. However this is expected to be extremely small and the edge X-ray spectrometer and charge exchange diagnostics will be used to determine this.

X-ray crystal spectrometers on current machines are based on the K-shell emission lines of helium like ions — argon, iron, titanium and nickel have been used, mostly chosen according to whether the electron temperature achiev-

able can ionize to this stage. The original design study for the ITER instrument [1] used the H- and He-like lines from krypton as its preferred observable. This choice envisaged the active introduction of krypton to make the measurement possible. Although actively introducing an extrinsic impurity can guarantee a measurement it can be preferable, for operational reasons, to rely on emission from intrinsic impurities. For ITER the only options are tungsten and iron. Figure 2.3 shows the radial emission profiles of the usable lines.

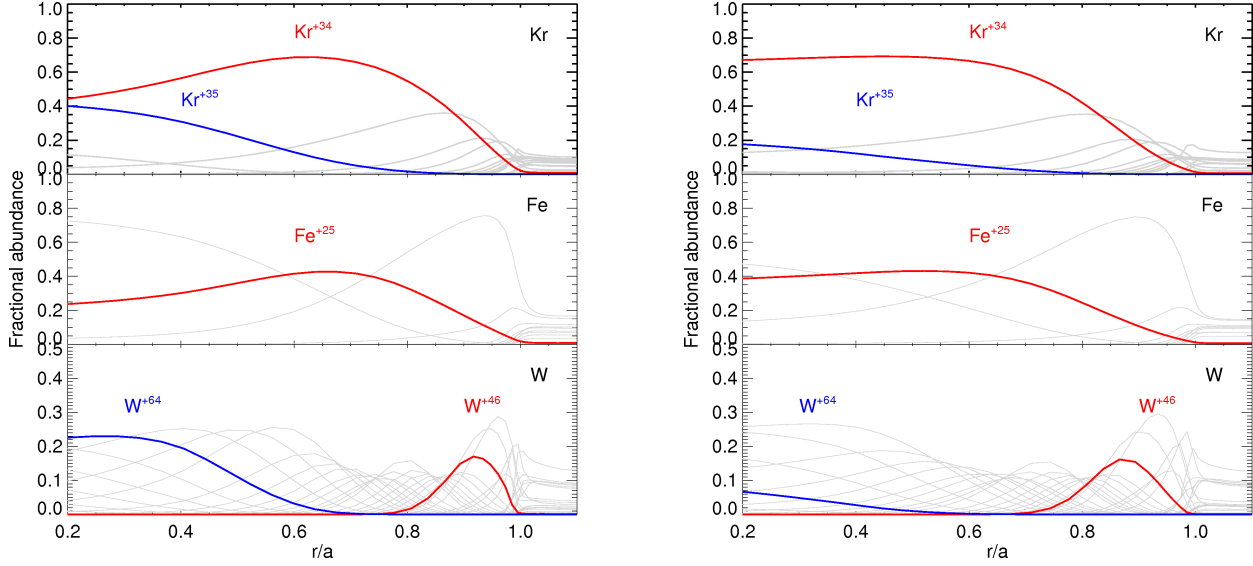


Figure 2.2: The radial location of emission from suitable X-ray lines of krypton, iron and tungsten in high performance (left) and lower power (right) ITER plasmas.

The lower performance plasma does not affect the usability of iron and krypton but deep core ion temperature measurements will be adversely affected by the lack of tungsten emission. This is more clearly seen by mapping the abundance along the extremes of each spectrometer onto the radial profile. Figure ?? illustrates the compromise associated with relying on impurity emission: the plasma conditions dictate the location of the measurement which means that in the lower performance plasmas the edge in temperature may become a more difficult measurement as the tungsten emission line used move further into the plasma following its temperature of maximum abundance.

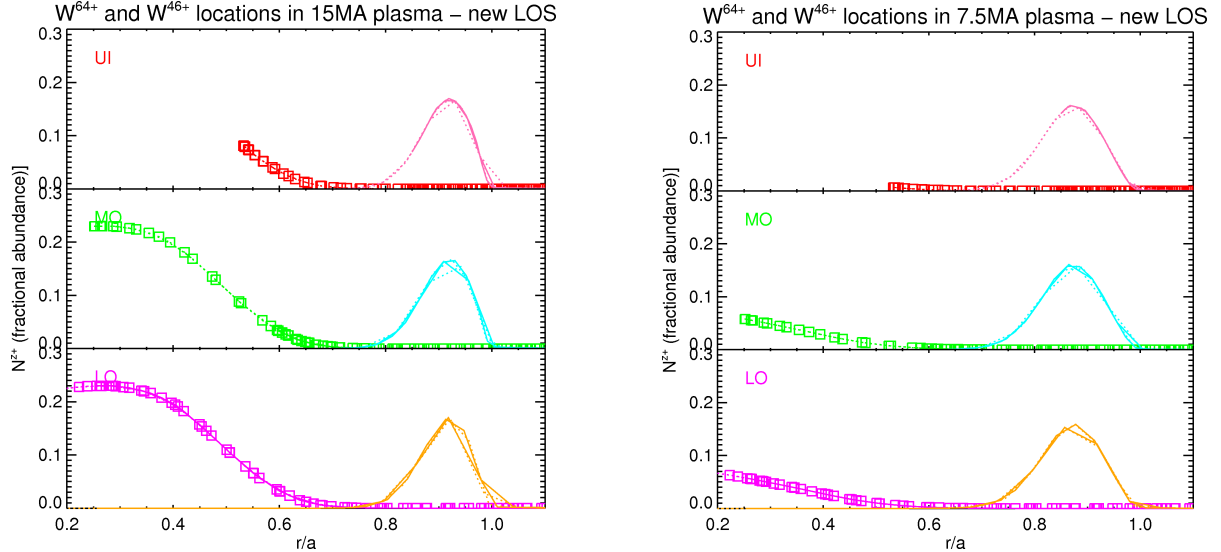


Figure 2.3: The abundance of the Ne-like and Ni-like mapped onto the poloidal mid-plane for high performance (left) and lower power (right) ITER plasmas.

To fully characterize the possible transitions the angular sweep of the integrated emission is shown for He-like krypton and Ni-like tungsten in figure 2.4. Allowing the capability to use krypton as an alternative if the intrinsic tungsten emission does not provide sufficient signal is prudent.

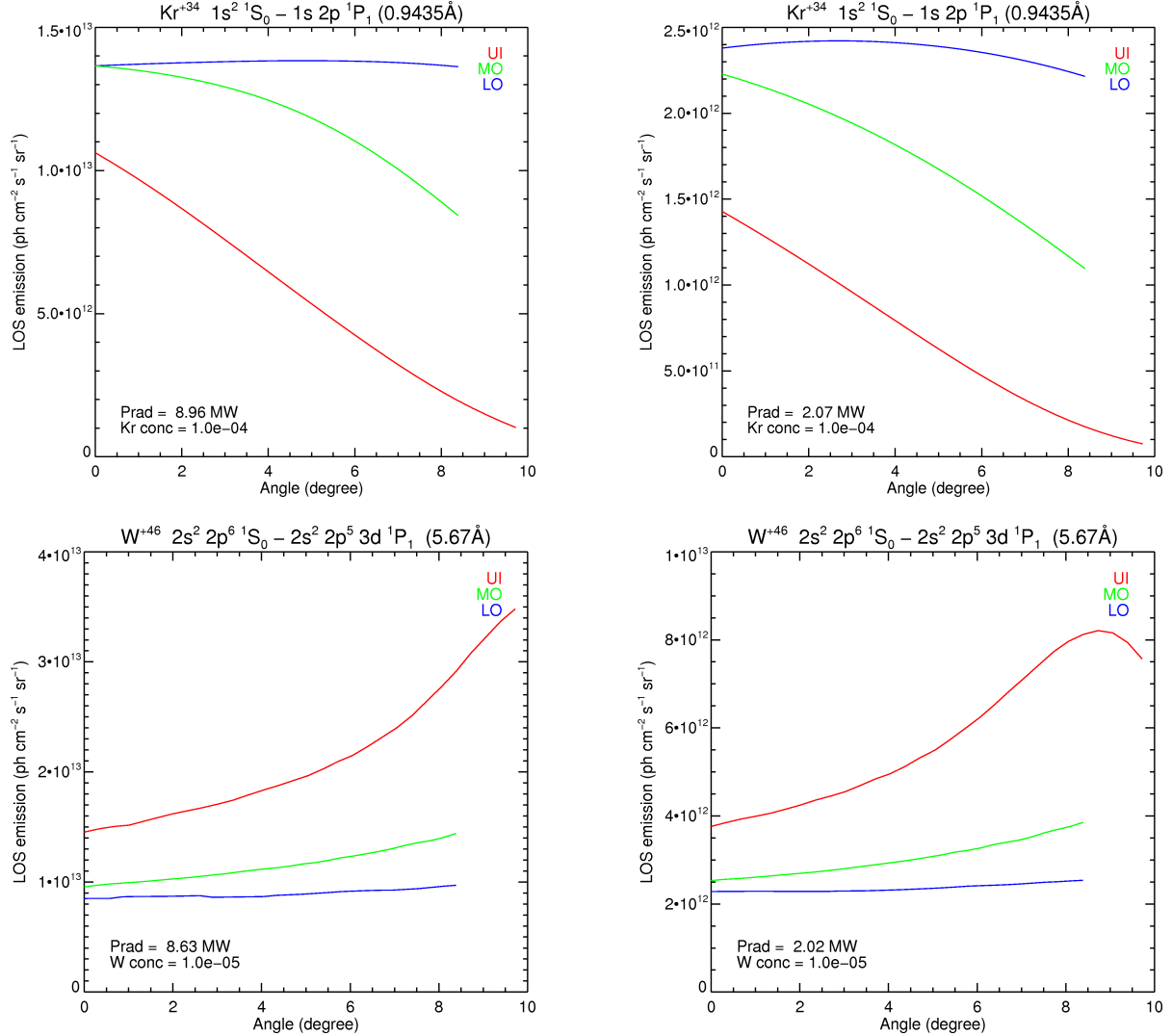


Figure 2.4: The angular variation for the 3 spectrometers for He-like krypton (top) and Ni-like tungsten (bottom) X-ray emission. The high performance plasmas are (left) with a lower power model (right).

These emission predictions formed part of the wider scope CDR, where choice of transitions also depend on operational, technological and environmental considerations.

Chapter 3

Bolometer

The radiation in ITER is emitted from all parts of the plasma. The fuel elements, hydrogen in the first phase and deuterium and tritium in the burning operation primarily give rise to continuum radiation. Any line radiation, which is significantly stronger than the continuum, at least for most anticipated ITER conditions, is dominated by line radiation.

Local plasma conditions, and transport, determine ion charge state. The bolometer system, which measures all the radiated power integrating across the full spectrum, will view emission representative of the core at 25keV and 10^{20} m^{-3} . as well as the divertor and edge region will can range from 0.5eV to 1000eV. Part of the design requirements is that the radiation profile must be measured, that reliable tomographic reconstructions are possible and that localized regions and ionisation fronts may be distinguished.

Consequently the design of the system is such that there are very many, up to 200, lines of sight covering all part of the plasma (figure 3.1).

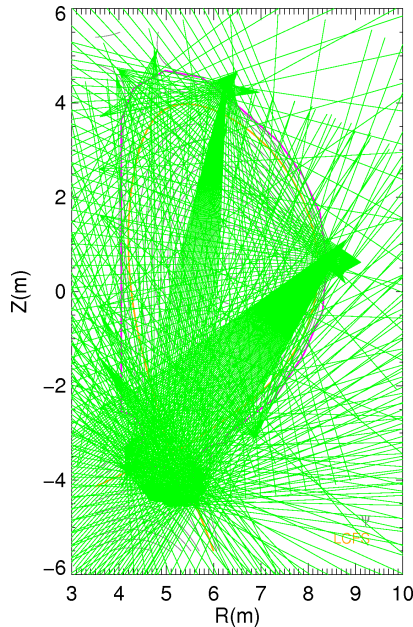


Figure 3.1: Lines of sight for bolometer. Typically 5 lines of sight are gathered within a case and the placement can be seen in the origin points of the various fans in the figure.

Forward modelling of the emission is required in order to determine the required response of the proposed bolometer detectors. The total line of sight integrated power influences the amount shielding, achieved by modifying the aperture, for each bolometer case enclosure in the system.

Since line radiation is the majority contributor to the emission any attenuating effects due to the material the bolometer is made from are significant. The bolometer is a simple bridge circuit with a platinum foil reacting to incident radiation. The potential signal is cut off below $\sim 10\text{eV}$ by reflections and above $\sim 20\text{keV}$ absorption effect start to become evident. Line emission from the principal impurities in ITER, are nearly all between these bounds. Figure 3.2 shows the energy response of a Pt foil, modelled after [2] and the energy of the prominent line of beryllium, tungsten and neon. The modification of the equilibrium radiated power response of iron is also shown. For practical purposes, the effects are small and do not alter any conclusions at the design phase. For interpreting measurements the correct response should be adopted in the analysis.

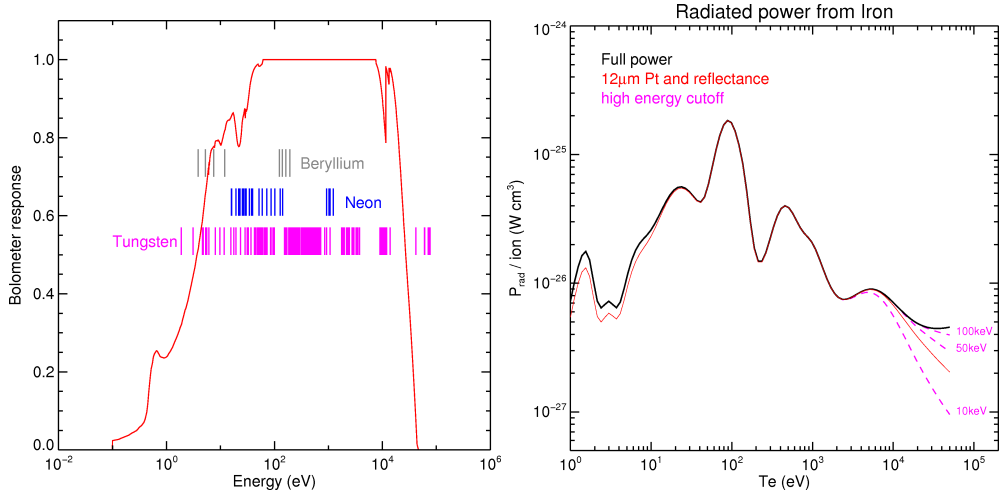


Figure 3.2: Nearly all line emission will be seen by the bolometer (left). High energy bremsstrahlung may be underestimated at very high temperatures if foil absorption effects are not considered (right).

Properly considering both the core and edge emission is important in modelling the bolometer signals. Two separate codes are used, SOPS for the edge and SANCO for the core. The former is, by necessity, 2D whereas the core transport can be properly described by a 1D, flux-average, model. Figure 3.3 shows the distribution of 0.4% neon radiation from these models.

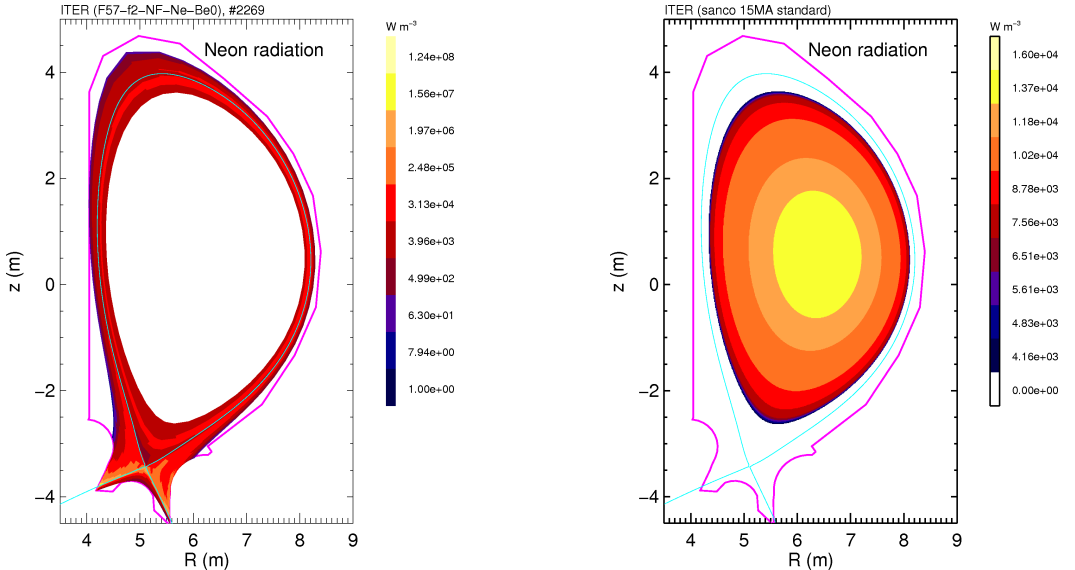


Figure 3.3: Neon radiation as predicted by 2D SOLPS (left) and 1D SANCO (right) transport models. These must be matched at their interface.

In the normal use of the 1D SANCO model the plasma is followed from the SOL to the core, with the proviso that the edge description is crude and possibly unphysical. This must be truncated to begin at the flux surface where the 2D SOLPS model shows a uniform plasma behaviour, ie where the flux-average picture is valid. The impurity density on this surface becomes the influx to the SANCO model. There should be continuity, and differential continuity, at this interface. In practice this condition is relaxed. Figure 3.4 shows the electron density profile along a horizontal line of sight and the background plasma adopted by the two transport codes. The standard 15MA reference core scenario for ITER and a high density SOLPS simulation are matched. The hybrid profile is used in the truncated SANCO run; in this example the matching (poloidal) normalized flux surface is at $\psi = 0.935$, which is beyond the pedestal region.

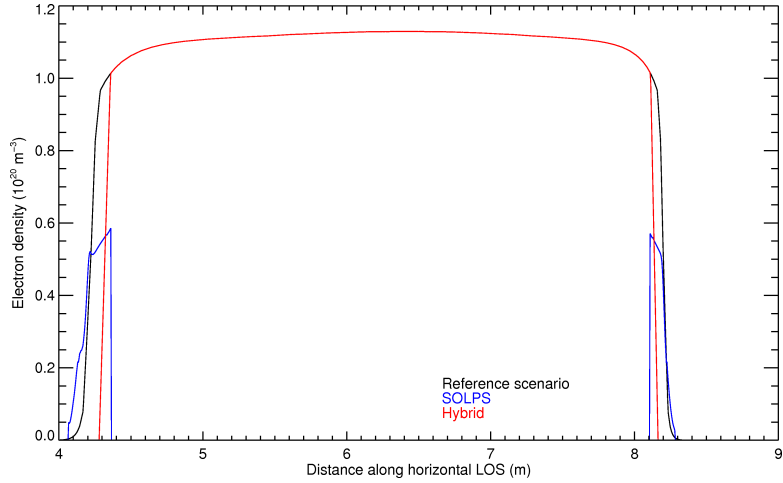


Figure 3.4: Electron density along a horizontal line of sight. The profiles are those used in the SOLPS (blue) and the truncated SANCO (red) code runs.

Line of sight integrated power predictions for the 15MA reference scenario with 0.4% neon were generated for all bolometer views. Figure 3.5 and table 3.1 gives a breakdown of the LOS power, into core and edge contributions and the fraction of the total from the neon impurity for two representative lines of sight.

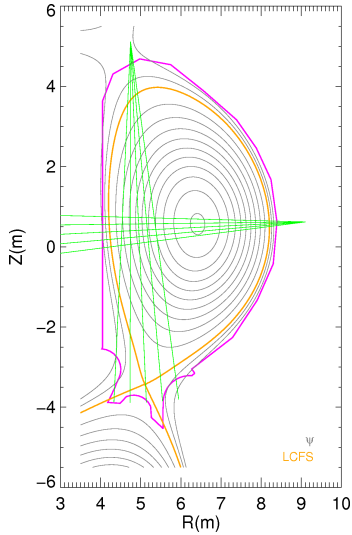


Figure 3.5: Equitorial port (#16, horizontal) and vertical port (#5) bolometer LOS.

	Pcore		Pedge		Neon/Total %
	Total (W cm ⁻²)	Neon (W cm ⁻²)	Total (W cm ⁻²)	Neon (W cm ⁻²)	
EPP #16	10.92	5.01	12.12	12.11	74.3
	10.92	5.01	12.11	12.10	74.3
	10.90	5.01	12.03	12.03	74.2
	10.85	4.98	12.07	12.06	74.3
	10.78	4.96	12.07	12.07	74.5
INVES #5	5.54	3.30	14.77	14.76	88.9
	8.41	4.70	14.75	14.75	83.9
	10.81	5.80	592.05	589.45	98.7
	12.63	6.54	657.21	653.52	98.5
	13.91	6.96	217.80	216.34	96.3

Table 3.1: Breakdown of radiated power for LOS in figure 3.5.

The contribution of neon to the overall radiation is ~75% in the core, confined plasma but this rises in the magnetically unconfined divertor plasma.

Another design driver is the ability to distinguish structures within the radiation emission. These can arise from heavy element asymmetric accumulation [3], interaction with the upper X-point or differently positioned ionisation fronts in the divertor. Figure 3.6 shows the radiation pattern for 3 simulations which vary just in the divertor density.

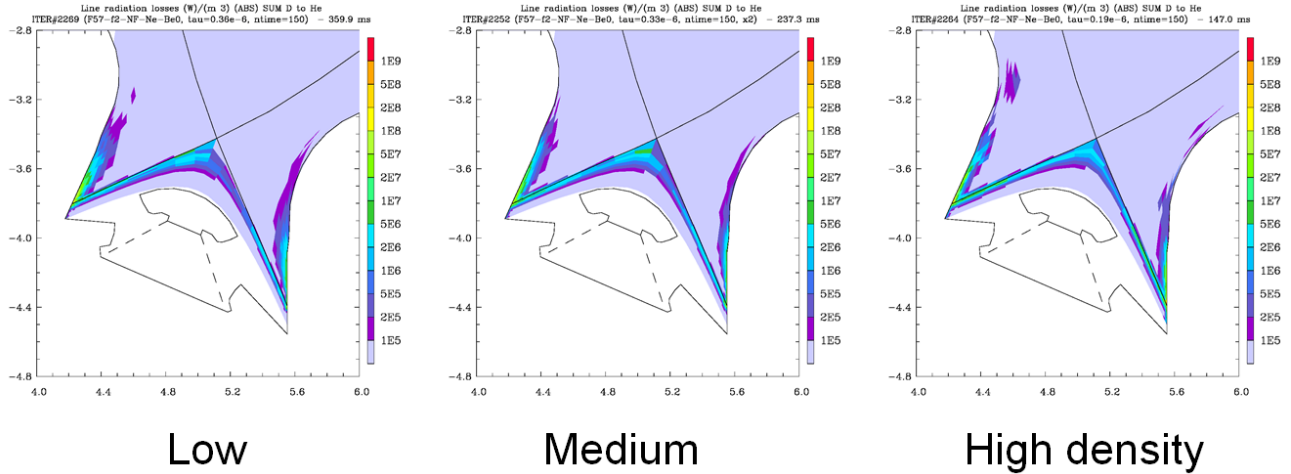


Figure 3.6: Total radiation from low, medium and high density divertor.

The equivalent LOS measurements are shown in figure 3.7 for two bolometer sensors located in the lower outer divertor.

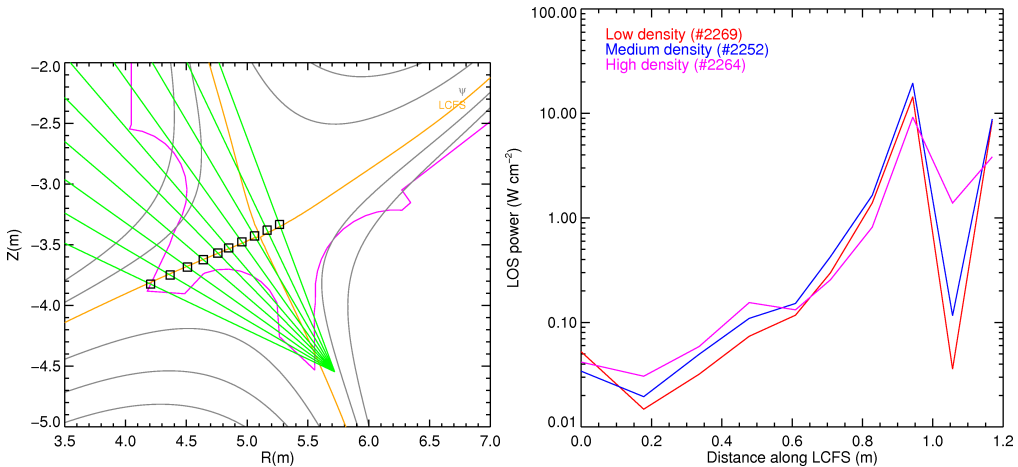


Figure 3.7: (left) Bolometer lines of sight covering the divertor assuming an unobstructed view through the gaps between the divertor cassettes. (right) Integrated radiated power from the low, medium and high density divertor simulations.

It can be concluded that this is a challenging measurements and that many lines of sight will be required to distinguish between the different possible scenarios.

More work needs to be done in order to complete the design study. In particular, a low power scenario characteristic of the start-up phase of ITER, is desirous. The effects of metals, and any poloidal asymmetries, must be modelled. The matching of the core and edge transport codes is *ad hoc* and must be made more rigorous.

Chapter 4

Divertor Impurity Monitor

The original design for the divertor impurity monitor (DIM) [4, 5] set out the lines of sight for the suite of instruments. There is extensive coverage of the inner and outer divertor legs via an innovative viewing system positioned under the divertor dome, thus removing any emission from the confined plasma. This system is complemented by wide angle views which image the divertor from an upper and a horizontal port; these instruments sample emission from the core and SOL plasma. The coverage is shown in figure 4.1.

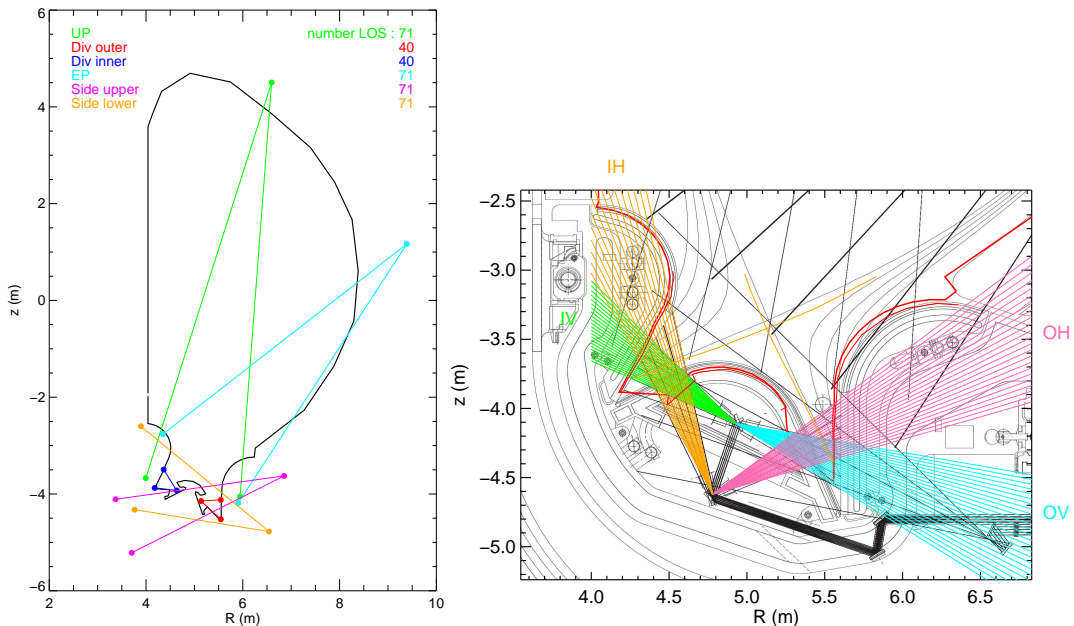


Figure 4.1: Overall coverage (top) and divertor leg views (bottom).

Comprehensive calculations for expected emission were reported in [6]. However this study assumed a carbon wall divertor and so no estimation of tungsten or beryllium emission was attempted. At the time of the CDR it was looking likely, and subsequently confirmed, that the ITER divertor would be made from tungsten and the first wall will be beryllium. There were some omissions which reduced its usefulness for the CDR: the forward predictions of emission were limited to one ITER plasma scenario, the use of representative lines of sight (LOS) within the divertor legs rather than those in the detailed design and no predictions were made for the wide angle upper and equatorial port views.

The spectrometers are designed to measure emission from 200–1000nm with 40 or 71 lines of sight:

Optical System	No. of Line of sight	Spot size of 0.2mm dia. Optical fiber at the Image plate	Measurement length (Image size)
EQ	71	40 ~ 50 mm	2160 mm
UP	71	40 ~ 50 mm	2020 mm
Div. Center (Inner)	40	20 mm	470 mm
Div. Center (Outer)	40	20 mm	470 mm
Div. Gap (Top)	71	30 ~ 40 mm	2200 mm
Div. Gap (Low)	71	30 ~ 40 mm	1900 mm

A number of emission line from beryllium, tungsten, helium and potential control gases of nitrogen, neon and argon are considered. The spectrometers will measure visible light so the choice of transitions are from neutral and singly ionized species.

Ion	λ (Å)	transition	adf15	exc	rec
BeI	2348	$2s\ 2p\ ^1P - 2s^2\ ^1S$	pec96#be_pju#be0.dat	1	24
	4573	$2s\ 3d\ ^1D - 2s\ 2p\ ^1P$		8	31
BeII	3130	$1s^2\ 2p\ ^2P - 1s^2\ 2s\ ^2S$	pec96#be_pju#be1.dat	1	22
	5270	$1s^2\ 4s\ ^2S - 1s^2\ 3p\ ^2P$		11	32
WI	4009	$5d^4\ 6s\ 6p\ ^7P_4 - 5d^5\ 6s\ ^7S_3$	pec#w_mons#w0ic.dat	1	
	5224	$5d^4\ 6s\ 6p\ ^7D_2 - 5d^4\ 6s^2\ ^5D_3$		2	
HeI	5875	$1s^2\ 3d\ ^3D - 1s^2\ 2p\ ^3P$	pec96#he_pju#he0.dat	9	24
	6678	$1s^2\ 3d\ ^1D - 1s^2\ 2p\ ^1P$		13	28
NII	5680	$2s^2\ 2p\ 3p\ ^3D - 2s^2\ 2p\ 3s\ ^3P$	pec96#n_vsu#n1.dat	3	53
NeI	6435	$2p^5(^2P_{1/2})\ 3s\ 0.5 - 2p^5(^2P_{3/2})\ 3s\ 1.5$	pec96#ne_pju#ne0.dat	7	26
ArI	6965	$3p^5\ 4p\ ^3P_1 - 3p^5\ 4s\ ^3P_2$	transport_llu#ar0.dat	8	

As the emission arises from the divertor and the edge plasma, a 2D emission model is required. For this the SOLPS [7] code is used: a fluid model of the parallel transport in the strongly collisional limit (including some kinetic corrections) with the kinetic Monte Carlo code Eirene [8] describing the neutral particle distribution. It has been used extensively in the design of the ITER divertor [9].

Impurity simulations have been run for three divertor densities, which were taken from the standard SOLPS density scan for Q=10 operation: 1537 ('low' density), 1514 ('medium') and 1538 ('high'). He, N, Ne, and Ar are assumed to be fully recycling, and the core concentrations are prescribed in line with the expected Z_{eff} . In addition, these runs were combined with two far-SOL plasmas that determine plasma-wall interaction in the main chamber: case *d* ('low' density far-SOL, with $T_e = 10$ eV) and case *o* ('high' density, $T_e = 20$ eV), where the far-SOL parameters are consistent with the ITER heat and nuclear loads specifications.

Scenario	Description
i-dib-0903-1537-00d	L-mode, low n, T=10
i-dib-0903-1537-00o	H-mode, high n, T=20
i-dib-0903-1514-00d	L-mode, low n, T=10
i-dib-0903-1514-00o	H-mode, high n, T=20
i-dib-0903-1538-00d	L-mode, low n, T=10
i-dib-0903-1538-00o	H-mode, high n, T=20

The line of sight emission is calculated by integrating the local emission along the line of sight calculated by combining the SOLPS electron and impurity densities with excitation and recombination photon emissivity coefficients taken from ADAS [10],

$$I = \frac{1}{4\pi} \int_{los} n_e(x) [n_z(x) \mathcal{PEC}^{exc}(x) + n_{z+1} \mathcal{PEC}^{rec}(x)] dx. \quad (\text{ph m}^{-2} \text{s}^{-1} \text{sr}^{-1})$$

Note that there is no recombination PEC data for the tungsten ions.

The SOLPS simulations are generated on a non-uniform grid of points so a line of sight is made up of many different length segments each characterized by a local electron temperature, electron density and impurity density distribution. The cells are optimized for the fluid code and may not be the preferred choice for diagnostic prediction.

Practically the integration is,

$$I = \frac{1}{4\pi} \sum_{i=1}^{cell} n_e(i) [n_z(i)\mathcal{PEC}^{exc}(i) + n_{z+1}\mathcal{PEC}^{rec}(i)] \Delta\ell(i)$$

where $\Delta\ell(i)$ is the intersection length of the LOS and the SOLPS cell. The electron and ionisation stage densities and PEC coefficients are constant in each cell.

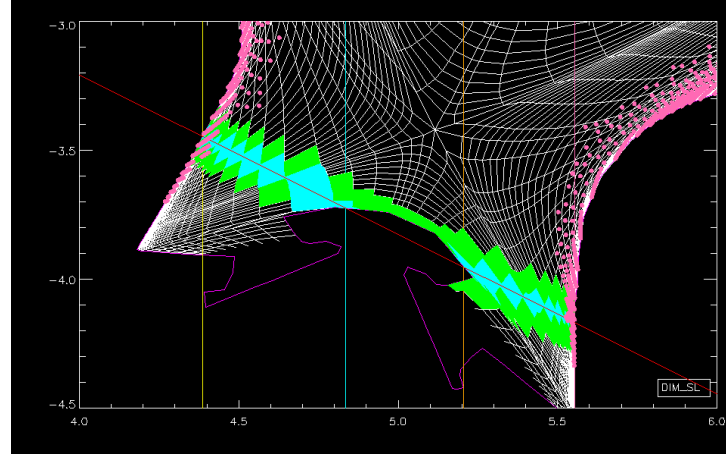


Figure 4.2: One (of 71) lines of sight for the divertor lower side view. See text for explanation.

Taking the divertor side lower view spectrometer as an example (figure 4.2), cells within 10cm are shown in green, there are 4 intersections with the wall but both inner and outer legs will be viewed through slits. The cyan cells are those with a non-zero intersection length. Finally the pink dots show where there is a finite W^0 density — in this case there is no emission in most of the cells along the LOS. The alternative integration method is to re-grid the SOLPS data onto a regular, rectangular grid but this causes anti-aliasing issues in the resulting integrals.

To test the integration method the LOS emission of carbon divertor simulations of [6] were taken as an independent implementation. The comparison of the LOS emissivity profiles from the under-dome spectrometers show differences — the overall shape is recovered but the magnitude varies by a factor of 3 or 30 depending on the spectral line chosen (figure 4.3). This discrepancy remains unresolved but it is unlikely that the shape would be offset by a constant amount,

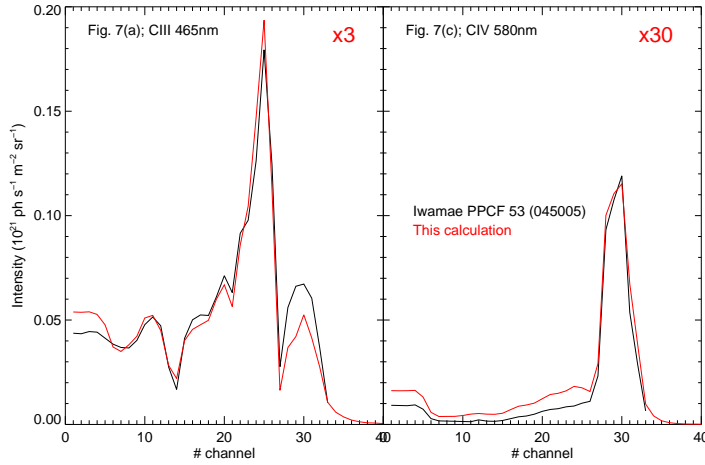


Figure 4.3: Adopted method of integration compared to results from [6].

across diverse plasma conditions, if the different integration methods did not agree.

The SOLPS simulations for the control gases are run assuming that one particle enters the system per second, per

metre toroidally. These are scaled to a 1% core concentration by the multiplier

$$f = \frac{1}{100} \sum_{ring17} \sum_z N_z / \sum_{ring17} Ne$$

where ring 17 is the ring of SOLPS cells just inside the separatrix. For the intrinsic plasma facing components (PFCs), ie Be and W, the concentrations are those calculated by the SOLPS simulations.

The results are presented as a table with a 2D image of the local emission followed by line integrated profiles as a function of the angular sweep of the six spectrometer views.

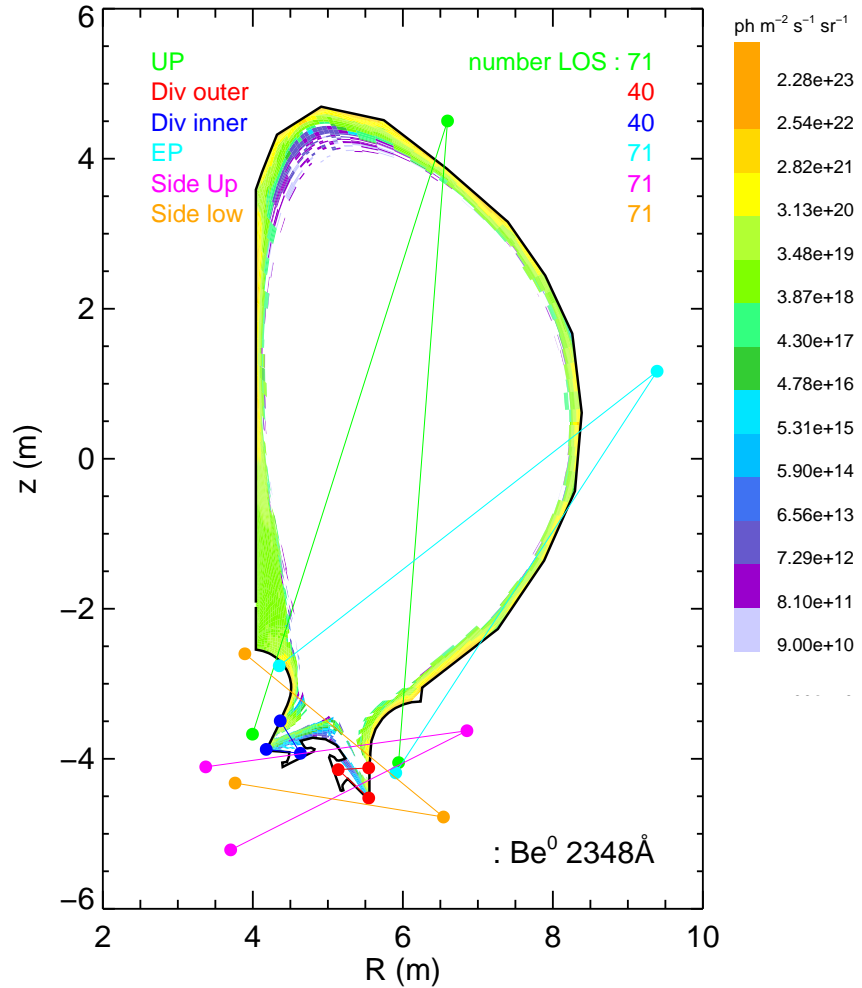
1. Eleven spectral lines in six SOLPS scenarios with emission profiles from 6 spectrometers are considered.
2. Concentrations of the intrinsic impurities are Be ($\sim 0.5\%$) and W (10^{-6}), which is low compared to contemporary machines. Extrinsic gases are normalized to 1% core concentration (ie $\int_0^{lcf_s} N_z(r)/N_e(r) = 0.01$).
3. The intrinsic impurities show a wider degree of variation between scenarios with the gases clearly showing the effect of the far-SOL temperature.
4. A wide variation in intensity along each profile make it difficult to reduce the predictions to a single figure of merit.

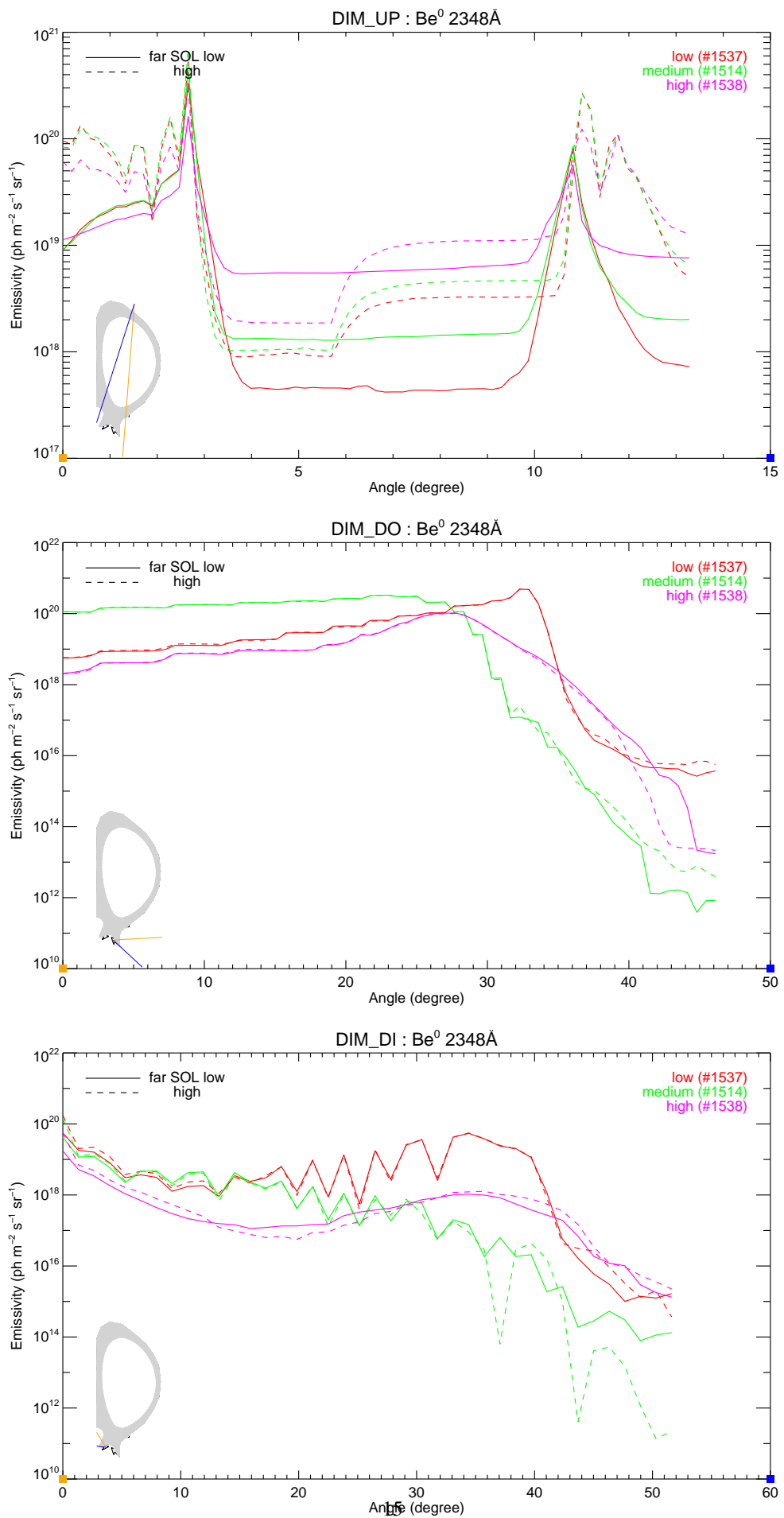
The emission profiles reflect the complexity of the divertor and all views are desirable to enable a full understanding of divertor radiation.

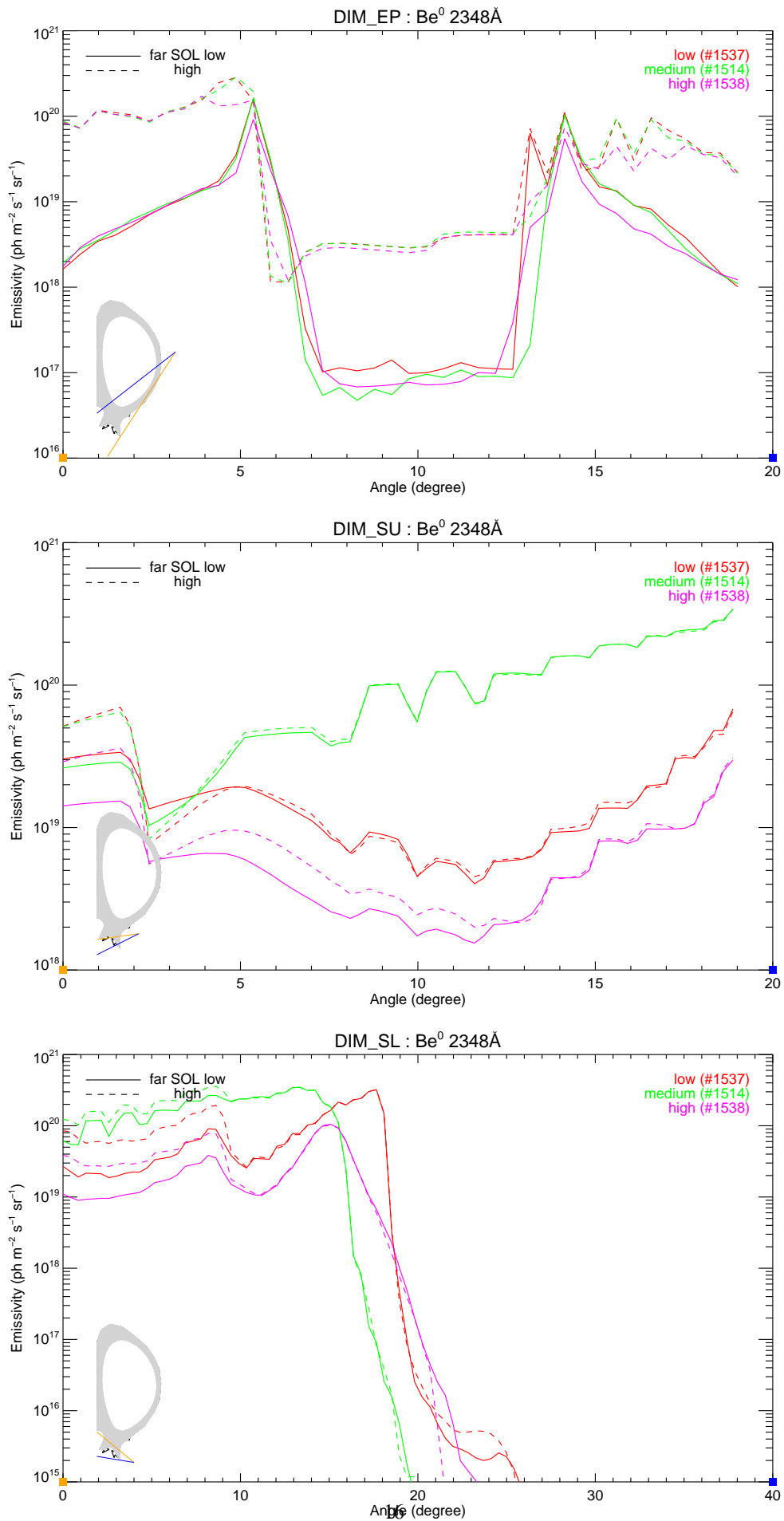
Be⁰ 2348Å, 2s 2p¹P – 2s² 1S

Summary of emission (in 10^{19} ph m $^{-2}$ s $^{-1}$ sr $^{-1}$) for the peak and minimum values and the LOS intensity at the centre point of the spectrometer fan and the value at the 75th percentile. The figure shows the poloidal distribution for scenario *i-dib-0903-1538-00o*.

Scenario conc. (%)	DIM_UP		DIM_DO		DIM_DI		DIM_EP		DIM_SU		DIM_SL	
	peak	min	peak	min	peak	min	peak	min	peak	min	peak	min
i-dib-0903-1537-00d (0.406)	33.270	0.043	48.876	6.474	5.591	1.776	16.063	0.010	6.800	0.826	32.084	16.458
i-dib-0903-1537-00o (0.790)	52.684	0.270	49.108	6.234	17.483	1.893	28.328	0.287	6.975	0.780	32.247	16.554
i-dib-0903-1514-00d (0.442)	43.467	0.136	32.865	32.865	4.208	0.095	16.123	0.008	34.090	10.127	34.620	18.616
i-dib-0903-1514-00o (0.822)	68.381	0.366	32.934	32.934	14.725	0.075	28.954	0.289	34.179	10.256	35.885	18.416
i-dib-0903-1538-00d (0.611)	16.160	0.569	10.432	3.872	1.741	0.038	9.159	0.008	2.979	0.239	10.540	10.540
i-dib-0903-1538-00o (0.571)	31.563	0.843	10.142	3.785	5.778	0.030	17.137	0.253	3.610	0.324	10.185	10.185
	0.186	4.713	0.000	1.796	0.000	0.104	0.122	8.767	0.200	1.032	0.000	3.835



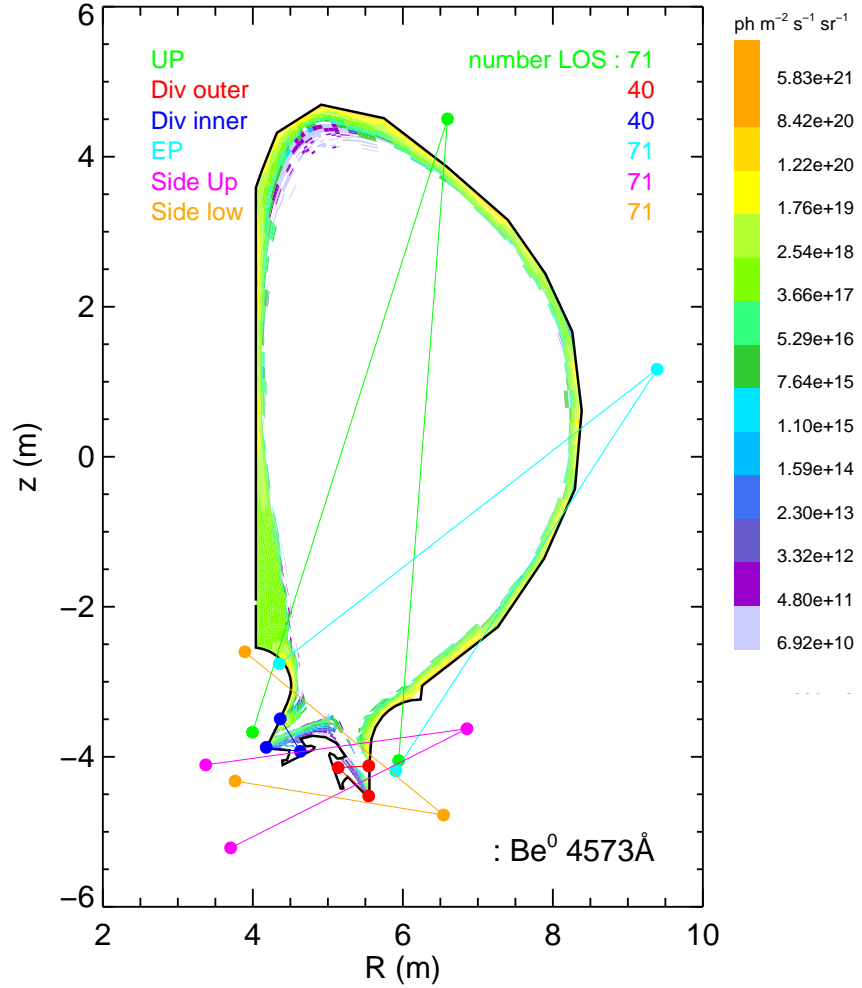


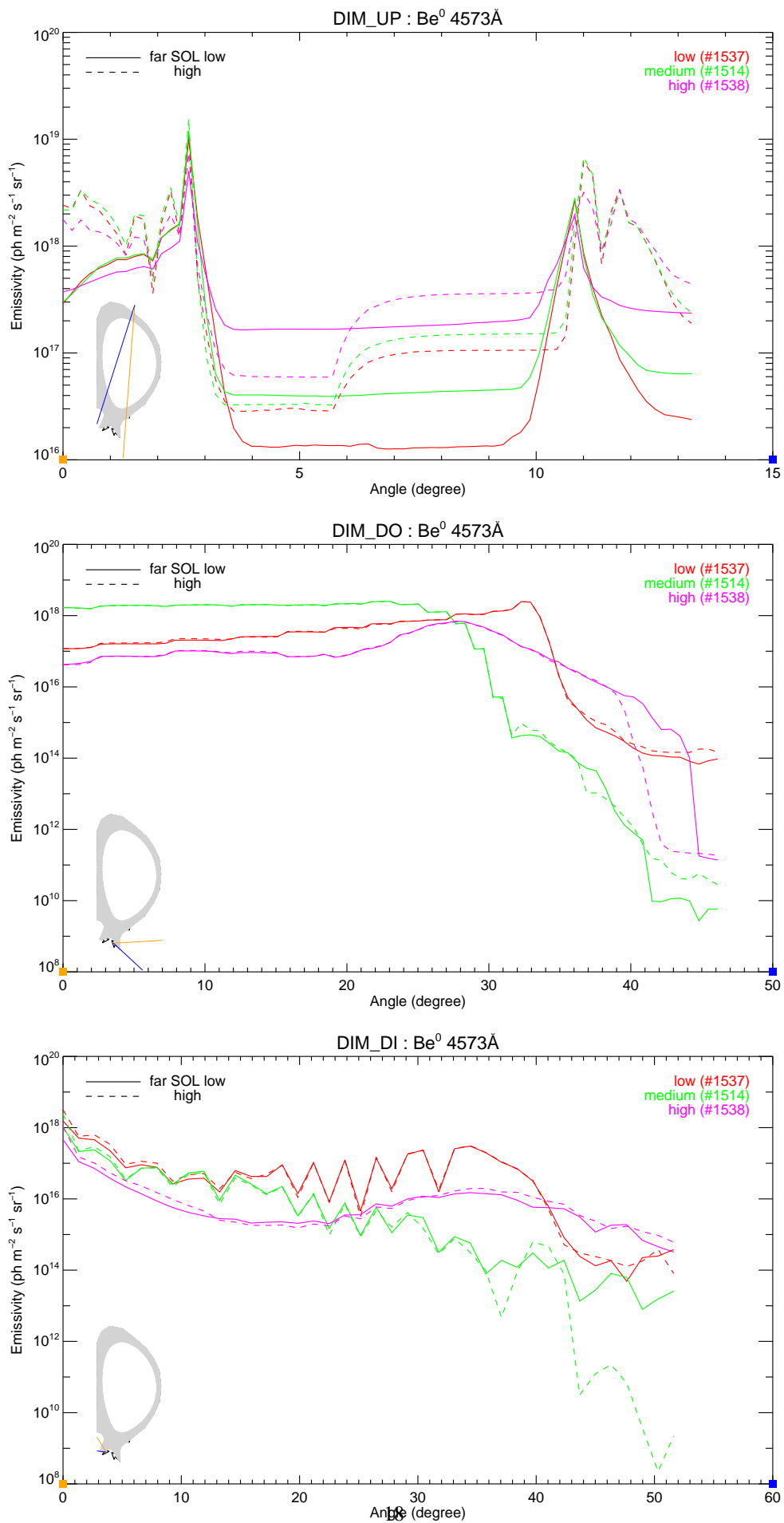


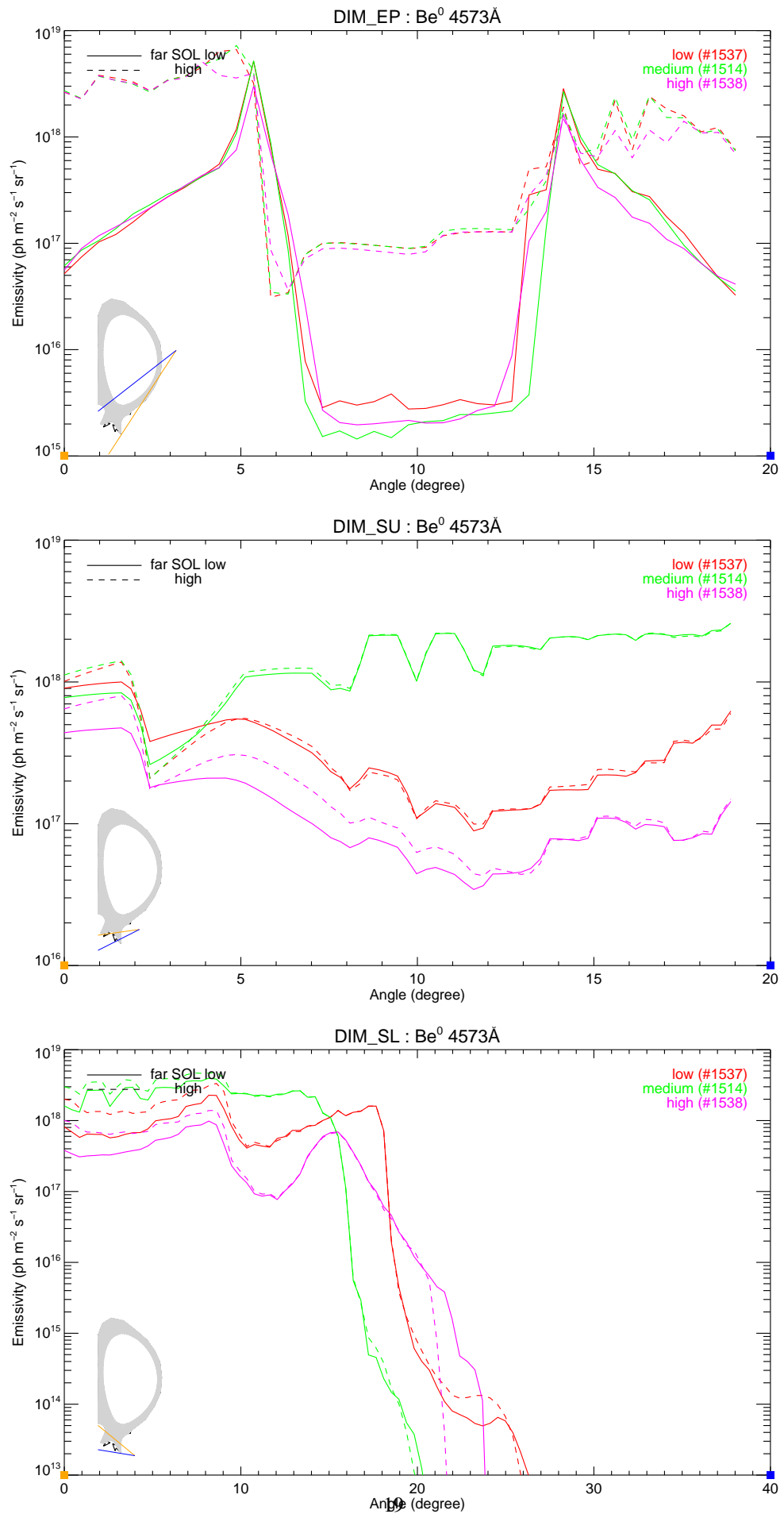
Be⁰ 4573Å, 2s 3d ¹D – 2s 2p ¹P

Summary of emission (in $10^{18} \text{ ph m}^{-2} \text{ s}^{-1} \text{ sr}^{-1}$) for the peak and minimum values and the LOS intensity at the centre point of the spectrometer fan and the value at the 75th percentile. The figure shows the poloidal distribution for scenario *i-dib-0903-1538-00o*.

Scenario conc. (%)	DIM_UP		DIM_DO		DIM_DI		DIM_EP		DIM_SU		DIM_SL	
	peak	min										
i-dib-0903-1537-00d (0.406)	10.038	0.013	2.465	0.592	1.546	0.139	5.144	0.003	1.000	0.217	2.283	1.114
i-dib-0903-1537-00o (0.790)	10.962	0.088	2.476	0.570	3.184	0.149	6.632	0.089	1.382	0.204	3.346	1.120
i-dib-0903-1514-00d (0.442)	11.924	0.041	2.497	2.497	1.053	0.006	5.193	0.002	2.592	2.131	3.962	1.107
i-dib-0903-1514-00o (0.822)	15.519	0.120	2.502	2.502	2.452	0.005	7.239	0.090	2.599	2.157	4.807	1.095
i-dib-0903-1538-00d (0.611)	5.011	0.173	0.698	0.178	0.462	0.007	3.005	0.002	0.474	0.068	0.984	0.676
i-dib-0903-1538-00o (0.571)	7.426	0.277	0.676	0.177	1.046	0.006	5.115	0.079	0.799	0.093	1.394	0.655
	0.059	1.230	0.000	0.124	0.001	0.016	0.037	2.715	0.043	0.259	0.000	0.686



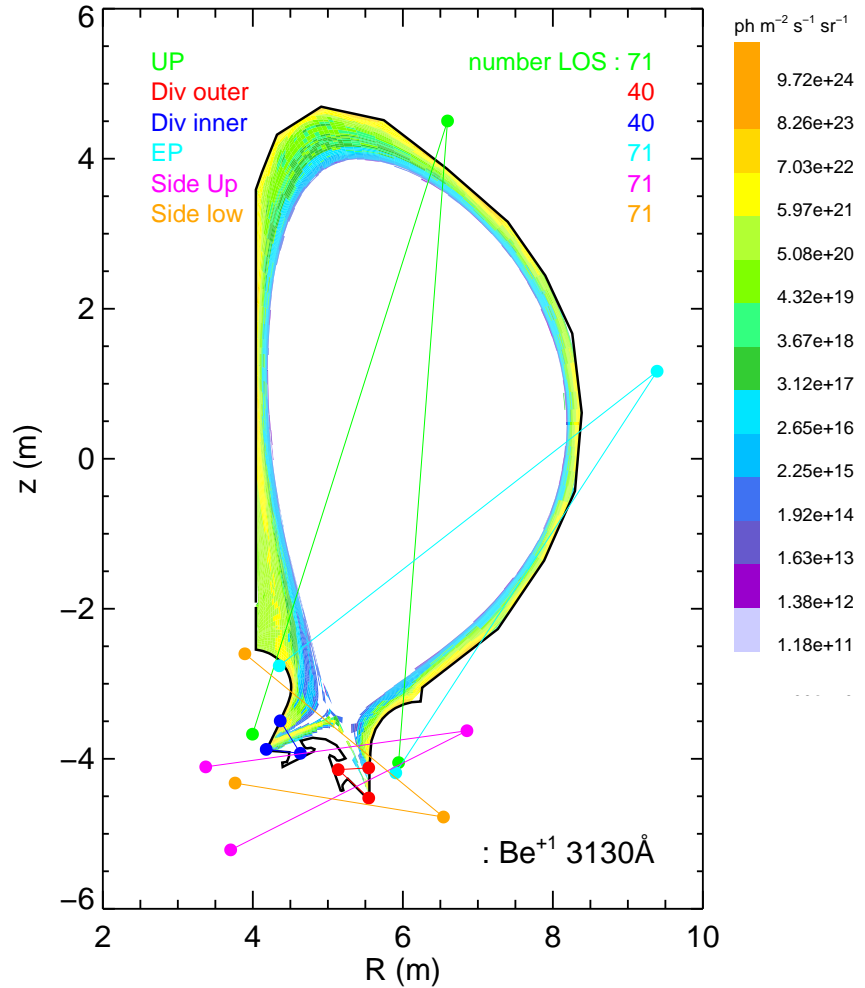


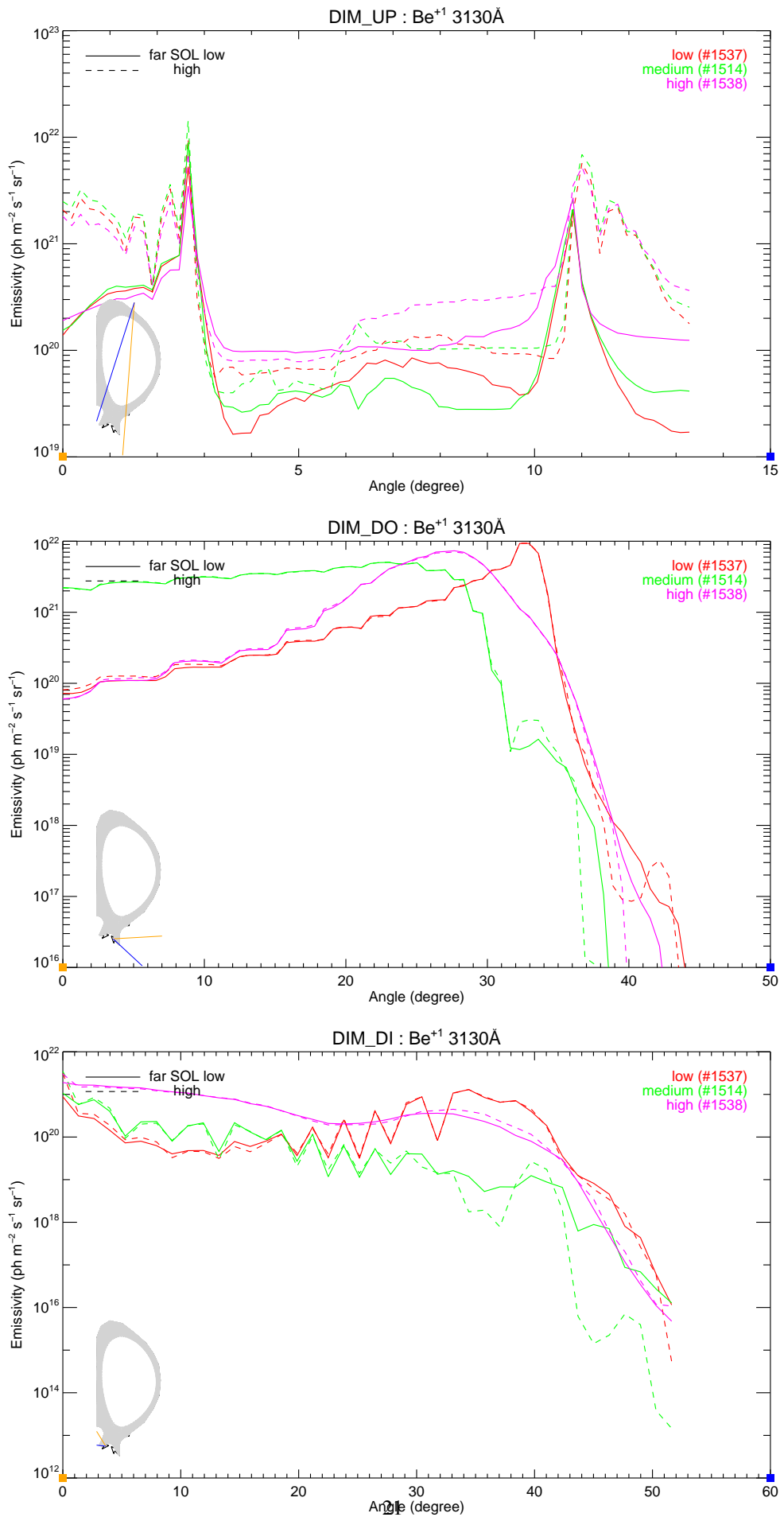


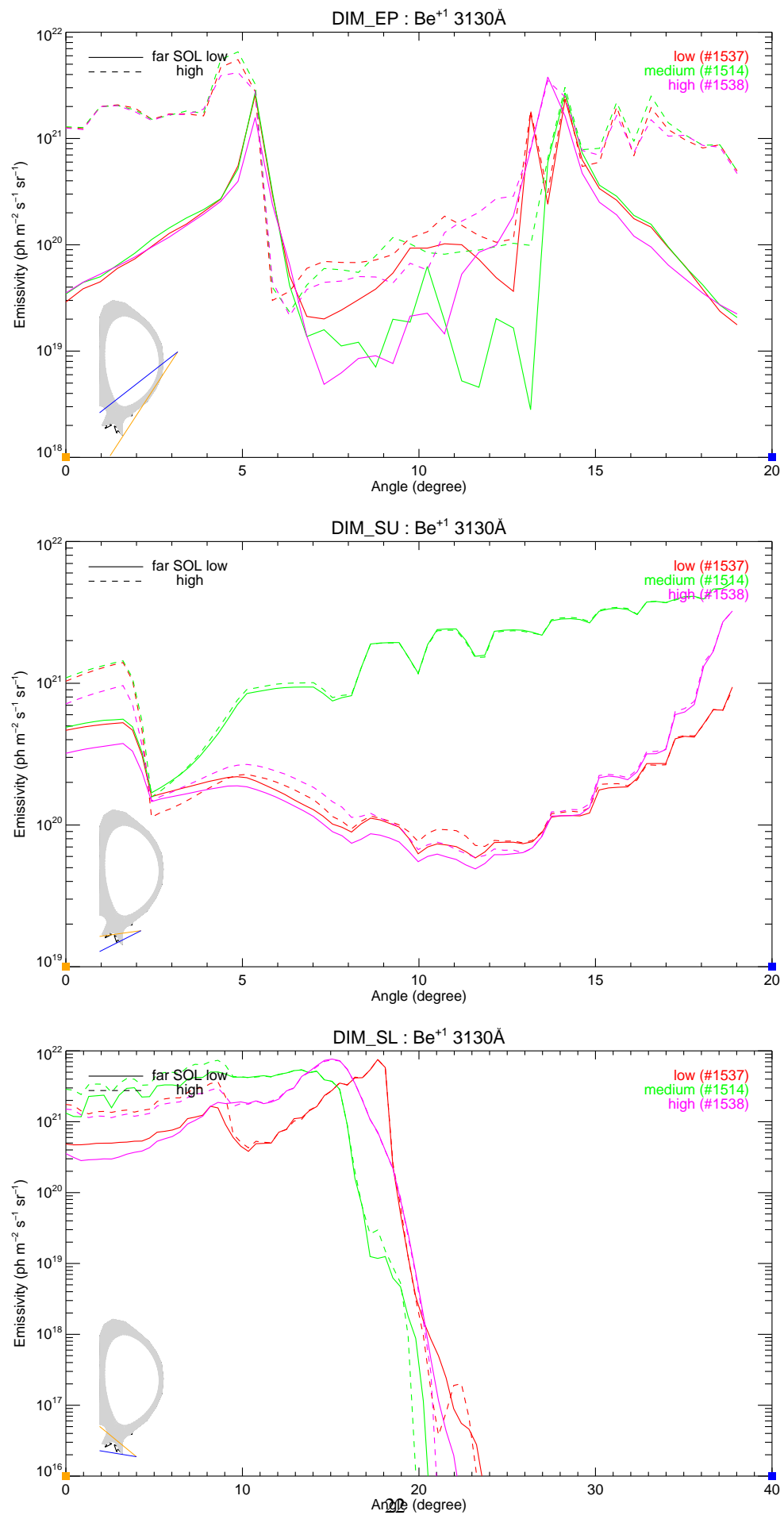
$\text{Be}^1 \text{ 3130\AA}$, $1s^2 2p\ ^2P - 1s^2 2s\ ^2S$

Summary of emission (in $10^{21} \text{ ph m}^{-2} \text{ s}^{-1} \text{ sr}^{-1}$) for the peak and minimum values and the LOS intensity at the centre point of the spectrometer fan and the value at the 75th percentile. The figure shows the poloidal distribution for scenario *i-dib-0903-1538-00o*.

Scenario conc. (%)	DIM_UP		DIM_DO		DIM_DI		DIM_EP		DIM_SU		DIM_SL	
	peak min	mid 75th	peak min	mid 75th	peak min	mid 75th	peak min	mid 75th	peak min	mid 75th	peak min	mid 75th
i-dib-0903-1537-00d (0.406)	5.277 0.016	0.075 0.257	9.327 0.000	0.902 1.144	1.297 0.000	0.409 0.399	2.555 0.018	0.093 0.241	0.940 0.059	0.097 0.271	7.530 0.000	2.775 1.106
i-dib-0903-1537-00o (0.790)	9.630 0.056	0.100 1.413	9.395 0.000	0.869 1.153	3.114 0.000	0.425 0.425	5.514 0.030	0.116 1.834	1.402 0.071	0.100 0.266	7.581 0.000	2.758 2.170
i-dib-0903-1514-00d (0.442)	8.898 0.026	0.045 0.264	5.045 0.000	5.045 3.673	1.070 0.000	0.053 0.145	2.720 0.003	0.019 0.214	5.154 0.169	1.938 2.838	5.380 0.000	3.725 4.216
i-dib-0903-1514-00o (0.822)	14.209 0.040	0.117 1.728	5.066 0.000	5.066 3.670	3.502 0.000	0.050 0.142	6.530 0.023	0.102 1.813	5.163 0.158	1.926 2.891	7.352 0.000	3.697 4.406
i-dib-0903-1538-00d (0.611)	3.477 0.095	0.108 0.283	7.333 0.000	4.092 1.813	1.903 0.000	0.227 0.935	3.789 0.005	0.021 0.194	3.234 0.049	0.076 0.318	7.662 0.000	7.662 1.853
i-dib-0903-1538-00o (0.571)	7.044 0.078	0.199 1.305	7.037 0.000	4.059 1.813	3.022 0.000	0.202 0.940	4.174 0.021	0.067 1.684	3.224 0.059	0.098 0.342	7.451 0.000	7.451 2.175



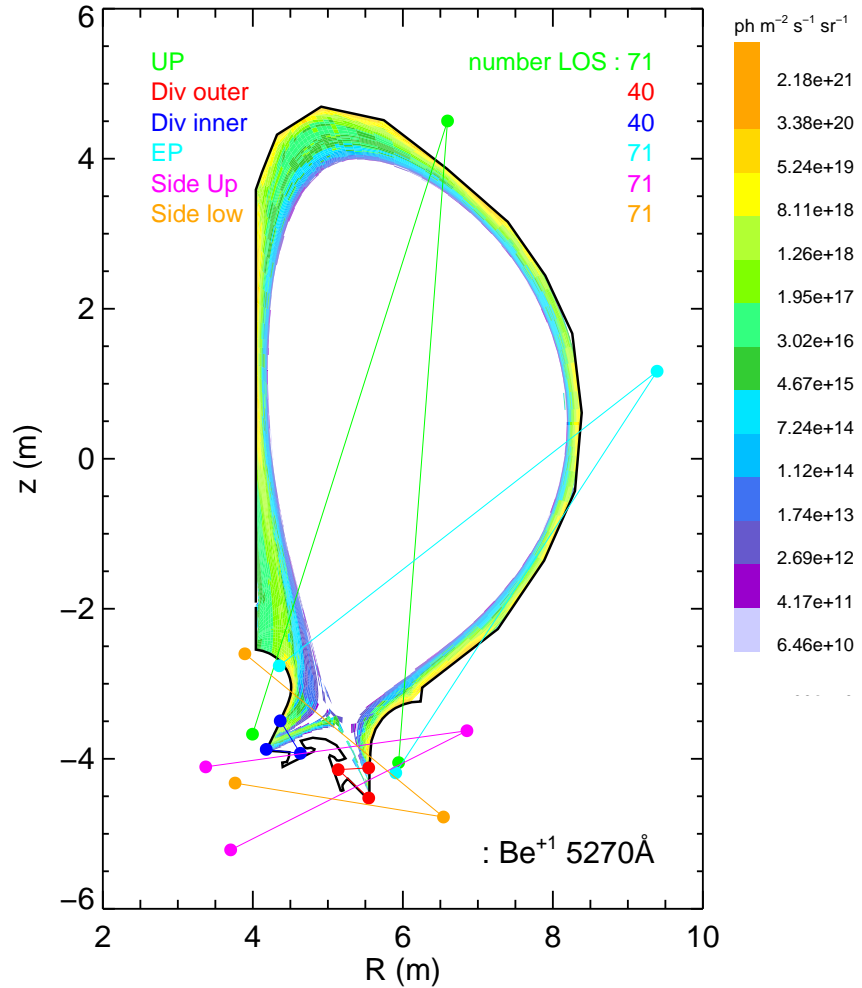


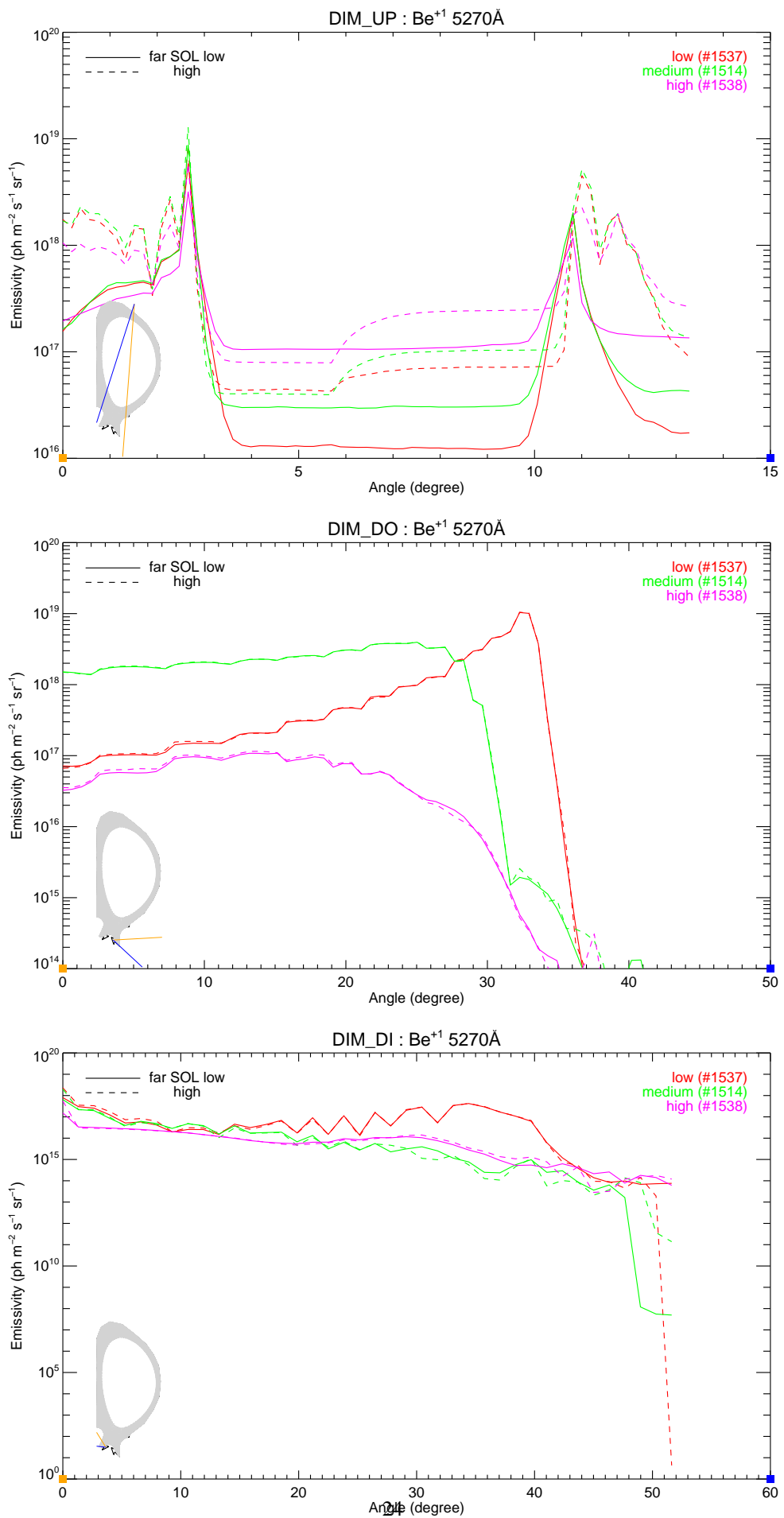


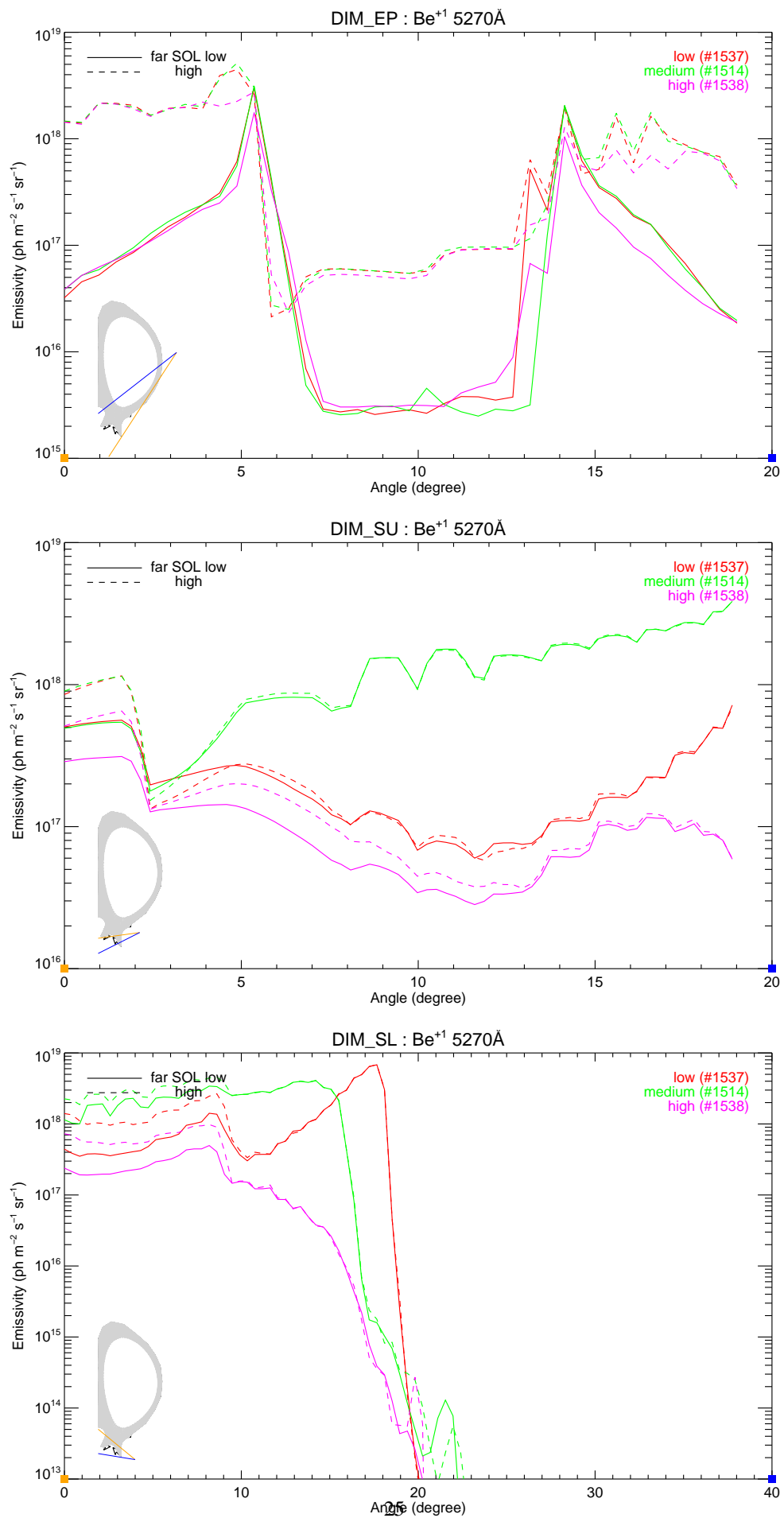
$\text{Be}^1 \text{ 5270\AA}$, $1s^2 4s \ ^2S - 1s^2 3p \ ^2P$

Summary of emission (in $10^{18} \text{ ph m}^{-2} \text{ s}^{-1} \text{ sr}^{-1}$) for the peak and minimum values and the LOS intensity at the centre point of the spectrometer fan and the value at the 75th percentile. The figure shows the poloidal distribution for scenario *i-dib-0903-1538-00o*.

Scenario conc. (%)	DIM_UP		DIM_DO		DIM_DI		DIM_EP		DIM_SU		DIM_SL	
	peak	min										
i-dib-0903-1537-00d (0.406)	5.843	0.013	10.369	0.687	0.802	0.160	3.000	0.003	0.717	0.111	6.814	1.861
i-dib-0903-1537-00o (0.790)	8.662	0.063	10.471	0.666	2.298	0.164	4.479	0.055	1.153	0.106	6.846	1.862
i-dib-0903-1514-00d (0.442)	8.730	0.030	3.956	3.789	0.646	0.006	3.141	0.003	3.858	1.544	4.067	3.080
i-dib-0903-1514-00o (0.822)	12.766	0.087	3.989	3.805	2.013	0.005	5.127	0.055	3.866	1.536	4.588	3.054
i-dib-0903-1538-00d (0.611)	3.185	0.106	0.108	0.054	0.153	0.011	1.760	0.003	0.312	0.046	0.497	0.026
i-dib-0903-1538-00o (0.571)	5.801	0.192	0.115	0.055	0.563	0.010	2.748	0.048	0.652	0.061	0.981	0.025
	0.079	0.894	0.000	0.086	0.000	0.015	0.023	1.624	0.037	0.172	0.000	0.540



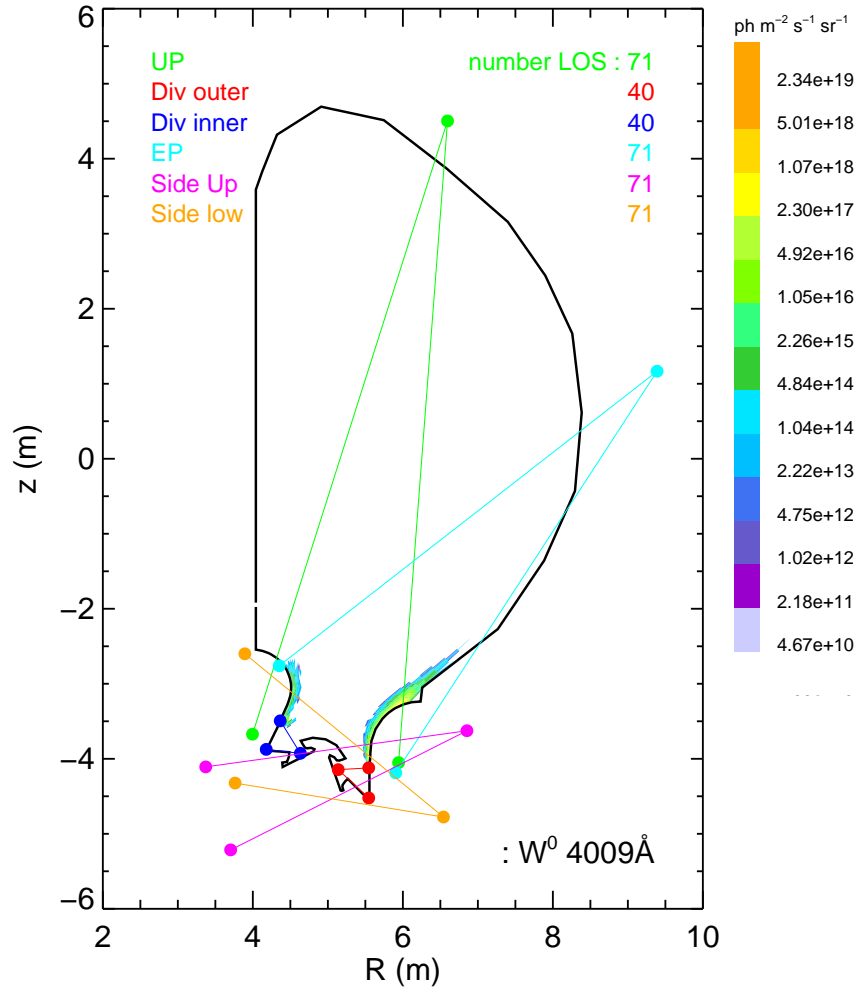


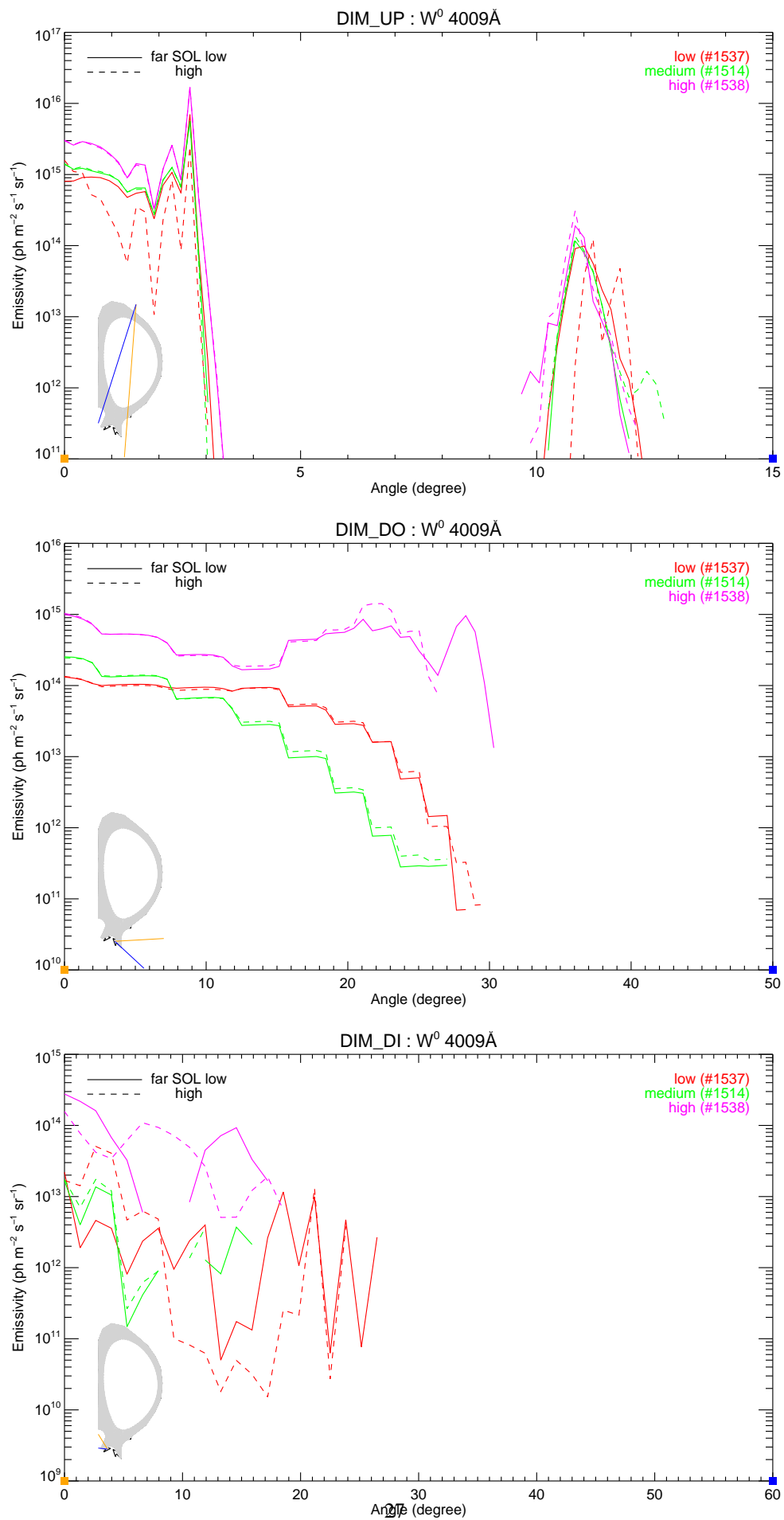


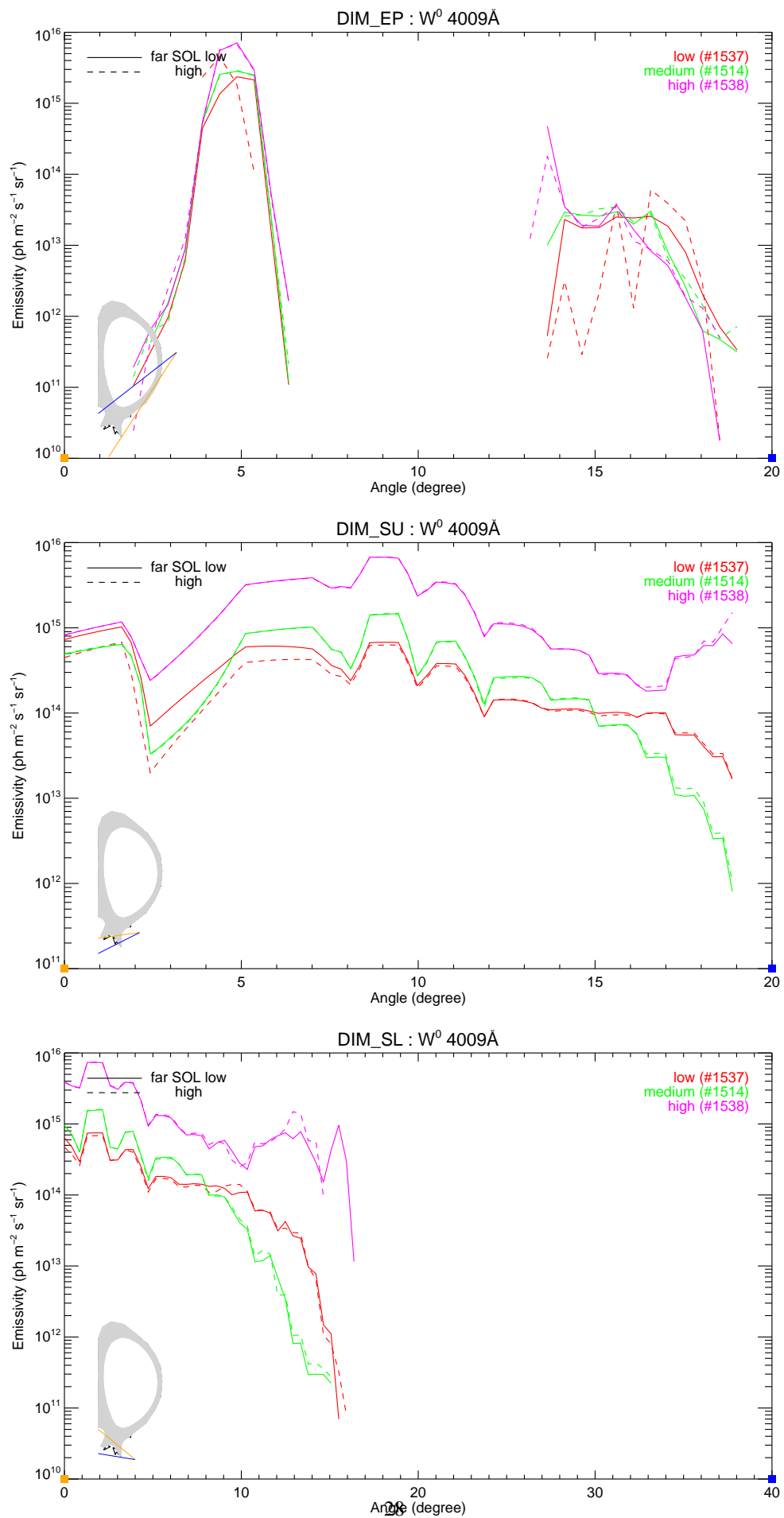
$W^0 4009\text{\AA}$, $5d^4 6s 6p \ ^7P_4 - 5d^5 6s \ ^7S_3$

Summary of emission (in $10^{15} \text{ ph m}^{-2} \text{ s}^{-1} \text{ sr}^{-1}$) for the peak and minimum values and the LOS intensity at the centre point of the spectrometer fan and the value at the 75th percentile. The figure shows the poloidal distribution for scenario *i-diw-0903-1538-00o*.

Scenario conc. (%)	DIM_UP		DIM_DO		DIM_DI		DIM_EP		DIM_SU		DIM_SL	
	peak	min	peak	mid								
i-diw-0903-1537-00d (0.0085)	6.984	0.000	0.132	0.016	0.022	0.003	2.362	0.000	1.025	0.673	0.750	0.001
i-diw-0903-1537-00o (0.0080)	2.467	0.000	0.134	0.016	0.051	0.000	4.566	0.000	0.680	0.626	0.688	0.001
i-diw-0903-1514-00d (0.0001)	5.600	0.000	0.254	0.001	0.017	0.000	2.824	0.000	1.456	1.456	1.586	0.000
i-diw-0903-1514-00o (0.0000)	5.647	0.000	0.245	0.001	0.017	0.000	2.890	0.000	1.475	1.475	1.609	0.000
i-diw-0903-1538-00d (0.0001)	16.766	0.000	0.997	0.691	0.277	0.000	7.095	0.000	6.748	6.556	7.377	0.428
i-diw-0903-1538-00o (0.0001)	16.835	0.000	1.422	1.146	0.157	0.000	6.815	0.000	6.760	6.607	7.383	0.000
	0.000	0.308	0.076	0.527	0.005	0.027	0.000	0.018	0.201	3.290	0.094	0.959



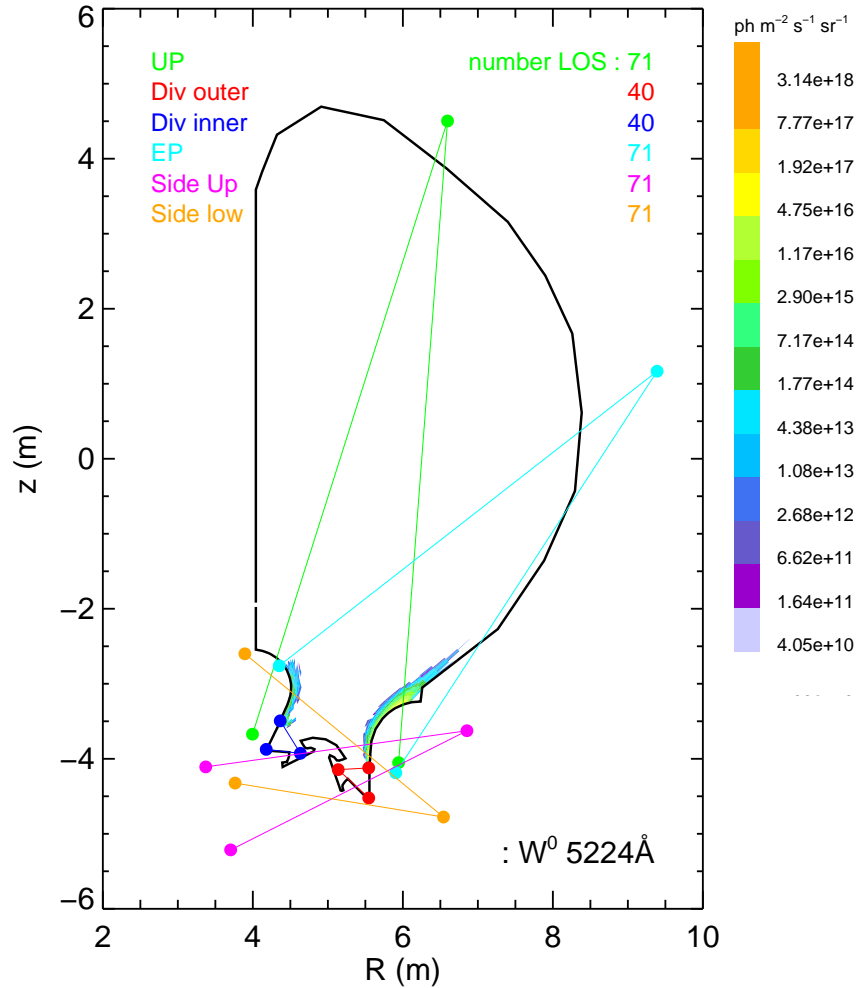


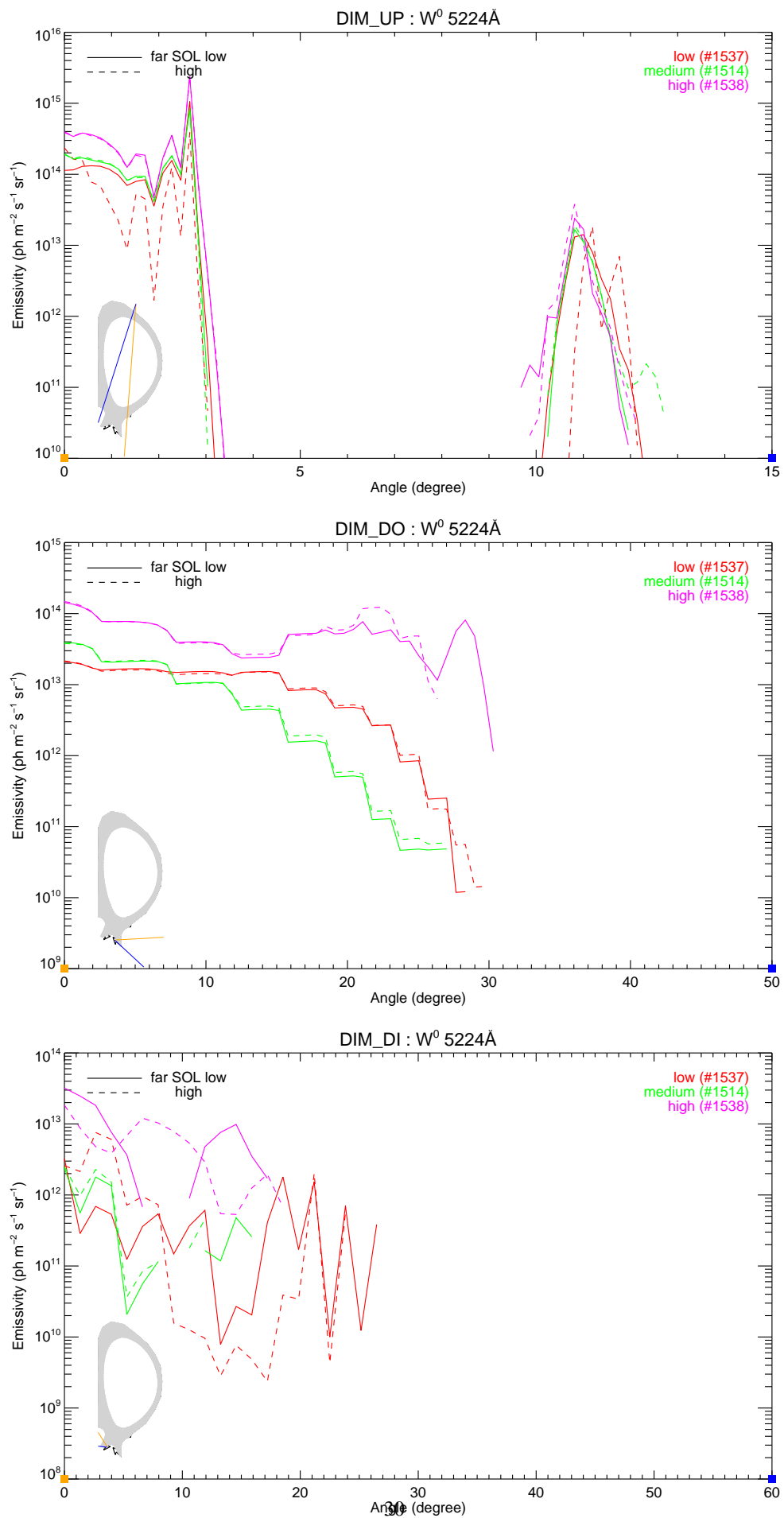


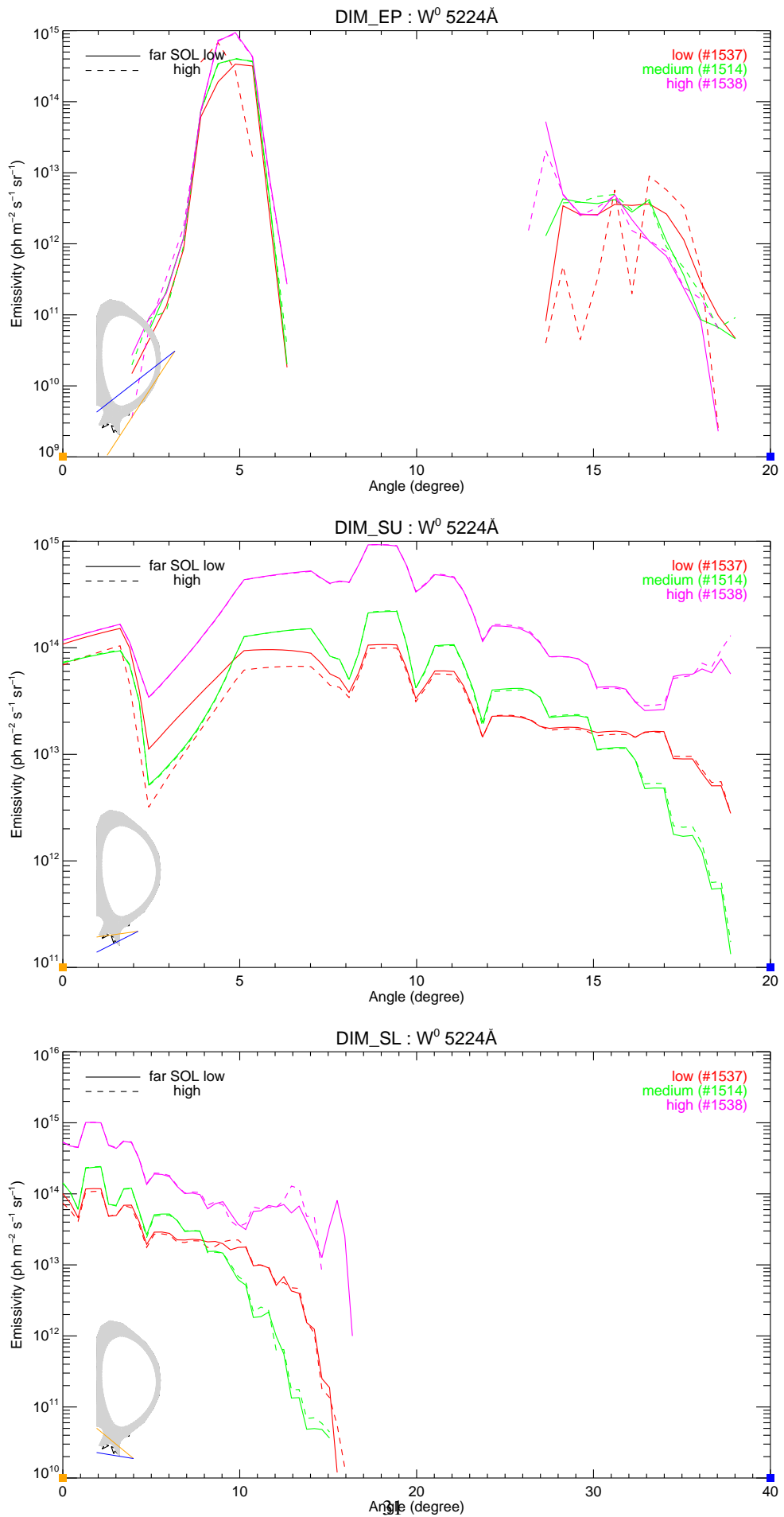
$W^0 \text{ 5224\AA}$, $5d^4 6s 6p \ ^7D_2 - 5d^4 6s^2 \ ^5D_3$

Summary of emission (in $10^{14} \text{ ph m}^{-2} \text{ s}^{-1} \text{ sr}^{-1}$) for the peak and minimum values and the LOS intensity at the centre point of the spectrometer fan and the value at the 75th percentile. The figure shows the poloidal distribution for scenario *i-diw-0903-1538-00o*.

Scenario conc. (%)	DIM_UP		DIM_DO		DIM_DI		DIM_EP		DIM_SU		DIM_SL	
	peak	min										
i-diw-0903-1537-00d (0.0085)	10.622	0.000	0.211	0.027	0.033	0.004	3.378	0.000	1.519	1.065	1.185	0.002
	0.000	0.131	0.000	0.152	0.000	0.004	0.000	0.026	0.028	0.941	0.000	0.225
i-diw-0903-1537-00o (0.0080)	3.880	0.000	0.215	0.027	0.076	0.000	6.785	0.000	1.044	0.991	1.088	0.001
	0.000	0.056	0.000	0.143	0.000	0.000	0.000	0.004	0.028	0.649	0.000	0.219
i-diw-0903-1514-00d (0.0001)	8.356	0.000	0.392	0.001	0.024	0.000	3.992	0.000	2.198	2.198	2.393	0.000
	0.000	0.110	0.000	0.104	0.000	0.001	0.000	0.037	0.001	1.046	0.000	0.297
i-diw-0903-1514-00o (0.0000)	8.425	0.000	0.378	0.002	0.025	0.000	4.085	0.000	2.227	2.227	2.428	0.000
	0.000	0.118	0.001	0.103	0.000	0.000	0.000	0.036	0.002	1.029	0.000	0.300
i-diw-0903-1538-00d (0.0001)	23.967	0.000	1.429	0.592	0.320	0.000	9.398	0.000	9.280	9.013	10.146	0.352
	0.000	0.239	0.012	0.577	0.007	0.017	0.000	0.025	0.258	4.507	0.010	1.026
i-diw-0903-1538-00o (0.0001)	24.073	0.000	1.479	0.978	0.184	0.000	9.030	0.000	9.295	9.084	10.153	0.000
	0.000	0.379	0.063	0.663	0.005	0.029	0.000	0.025	0.286	4.492	0.079	1.288



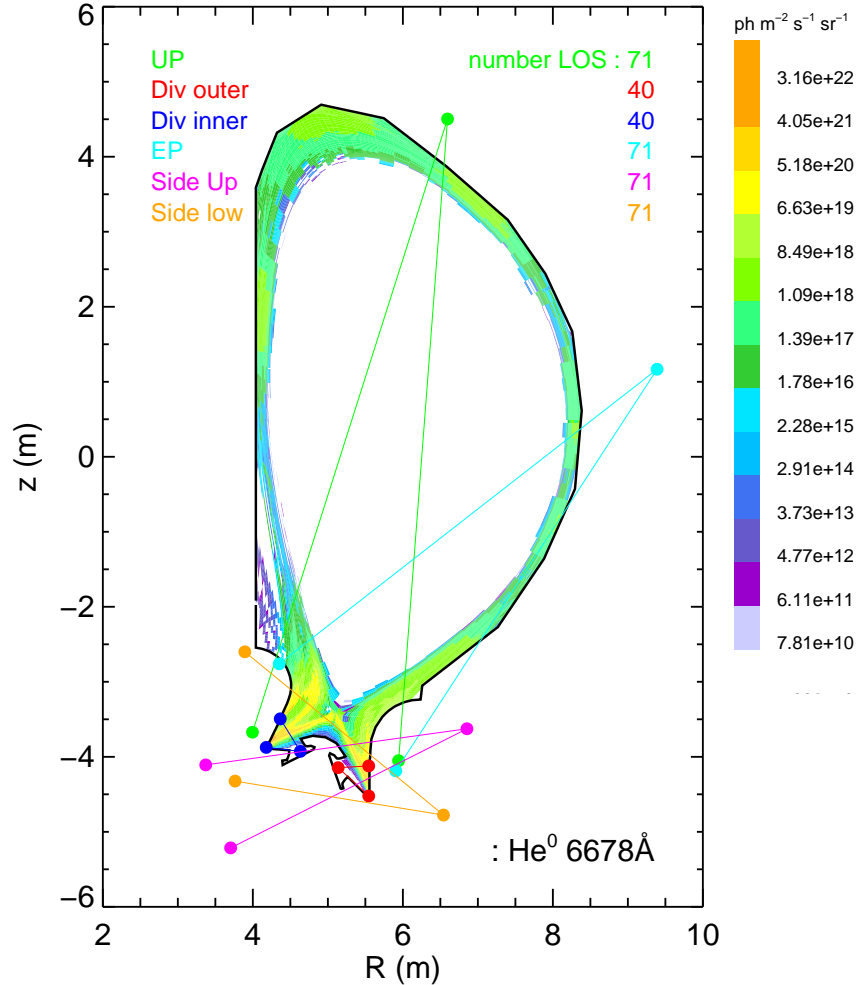


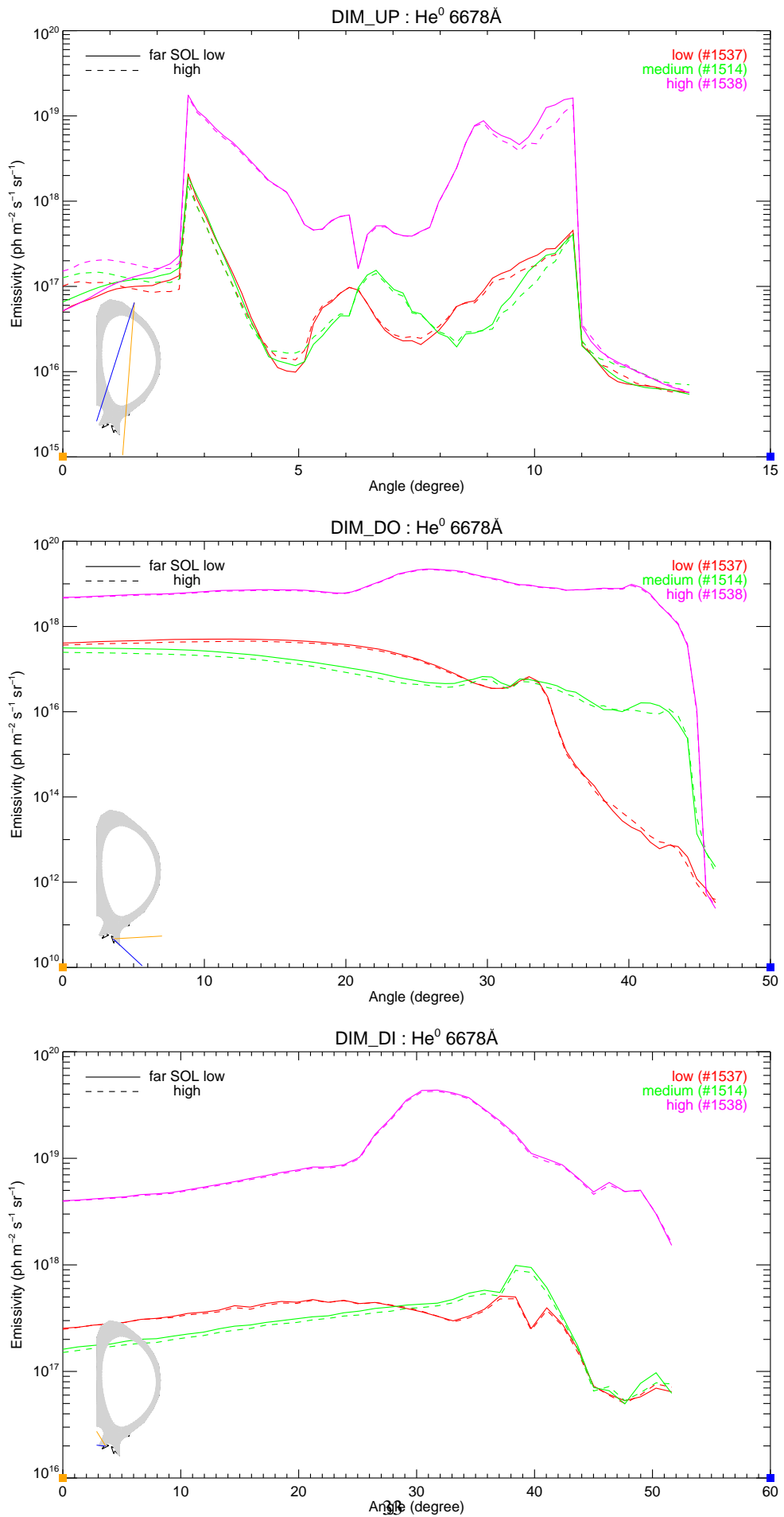


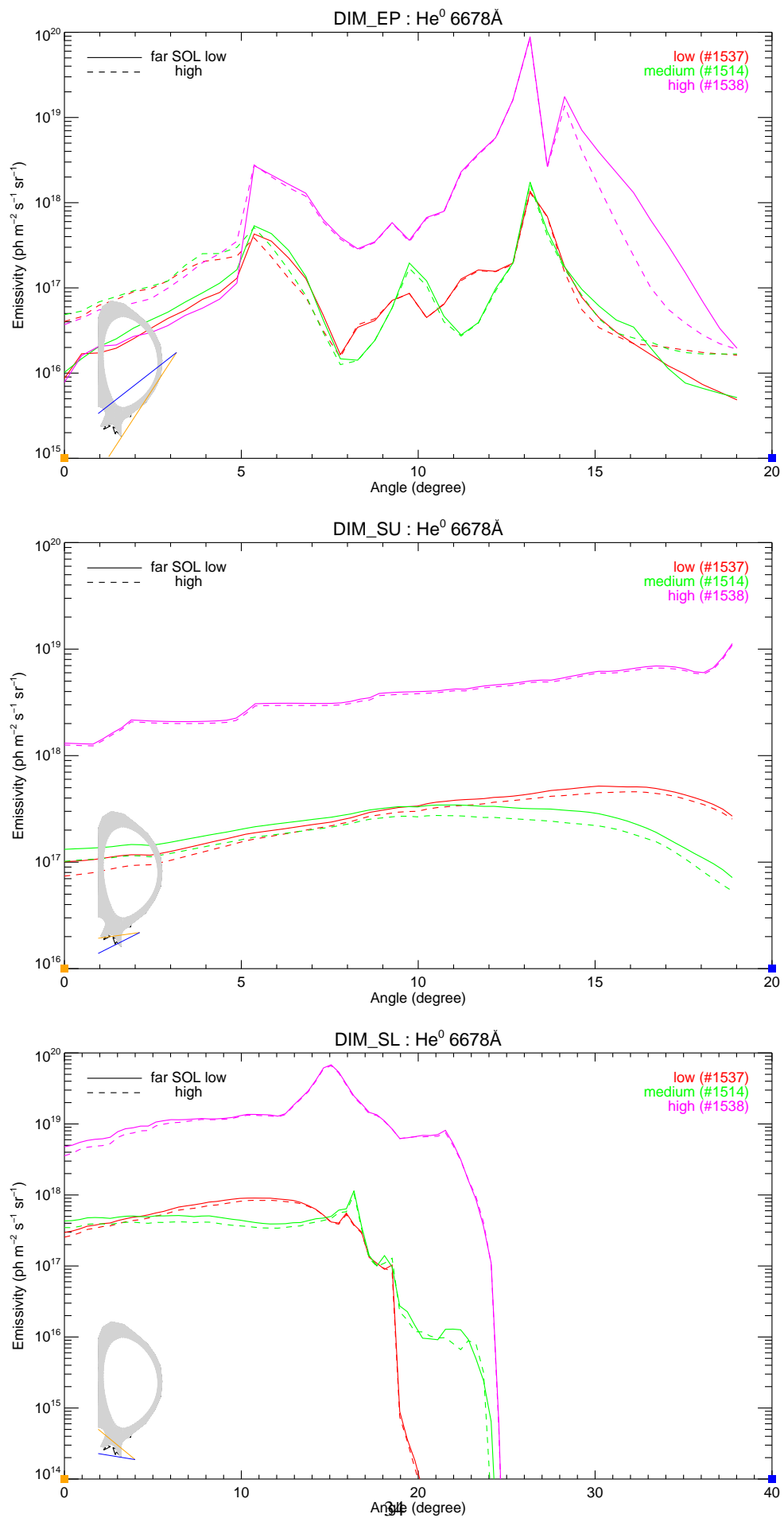
$\text{He}^0 \text{ 6678\AA}$, $1s^2 3d \ ^1D - 1s^2 2p \ ^1P$

Summary of emission (in $10^{18} \text{ ph m}^{-2} \text{ s}^{-1} \text{ sr}^{-1}$) for the peak and minimum values and the LOS intensity at the centre point of the spectrometer fan and the value at the 75th percentile. The figure shows the poloidal distribution for scenario *i-gas-0003-1538-00o*.

Scenario conc. (%)	DIM_UP		DIM_DO		DIM_DI		DIM_EP		DIM_SU		DIM_SL	
	peak min	mid 75th	peak min	mid 75th	peak min	mid 75th	peak min	mid 75th	peak min	mid 75th	peak min	mid 75th
i-gas-0003-1537-00d (1.0000)	2.091 0.006	0.042 0.125	0.505 0.000	0.260 0.466	0.509 0.053	0.444 0.434	1.358 0.005	0.086 0.130	0.518 0.101	0.326 0.429	0.904 0.000	0.417 0.702
i-gas-0003-1537-00o (1.0000)	1.820 0.006	0.044 0.111	0.453 0.000	0.240 0.412	0.482 0.050	0.445 0.421	1.310 0.015	0.086 0.159	0.458 0.074	0.295 0.393	0.842 0.000	0.409 0.632
i-gas-0003-1514-00d (1.0000)	1.917 0.005	0.155 0.127	0.315 0.000	0.071 0.260	0.989 0.050	0.390 0.419	1.749 0.005	0.196 0.136	0.344 0.072	0.332 0.317	1.147 0.000	0.500 0.490
i-gas-0003-1514-00o (1.0000)	1.504 0.007	0.142 0.127	0.248 0.000	0.053 0.201	0.889 0.053	0.356 0.390	1.655 0.013	0.170 0.170	0.274 0.054	0.270 0.252	1.033 0.000	0.466 0.406
i-gas-0003-1538-00d (1.0000)	17.540 0.006	0.513 4.876	22.270 0.000	13.793 9.569	43.691 1.526	16.819 16.712	88.307 0.008	0.362 2.296	11.270 1.283	3.940 5.748	68.119 0.000	68.119 13.423
i-gas-0003-1538-00o (1.0000)	16.899 0.006	0.493 4.649	21.544 0.000	13.358 9.143	42.574 1.609	16.351 16.119	85.721 0.019	0.348 2.013	10.904 1.235	3.754 5.529	66.223 0.000	66.223 12.991



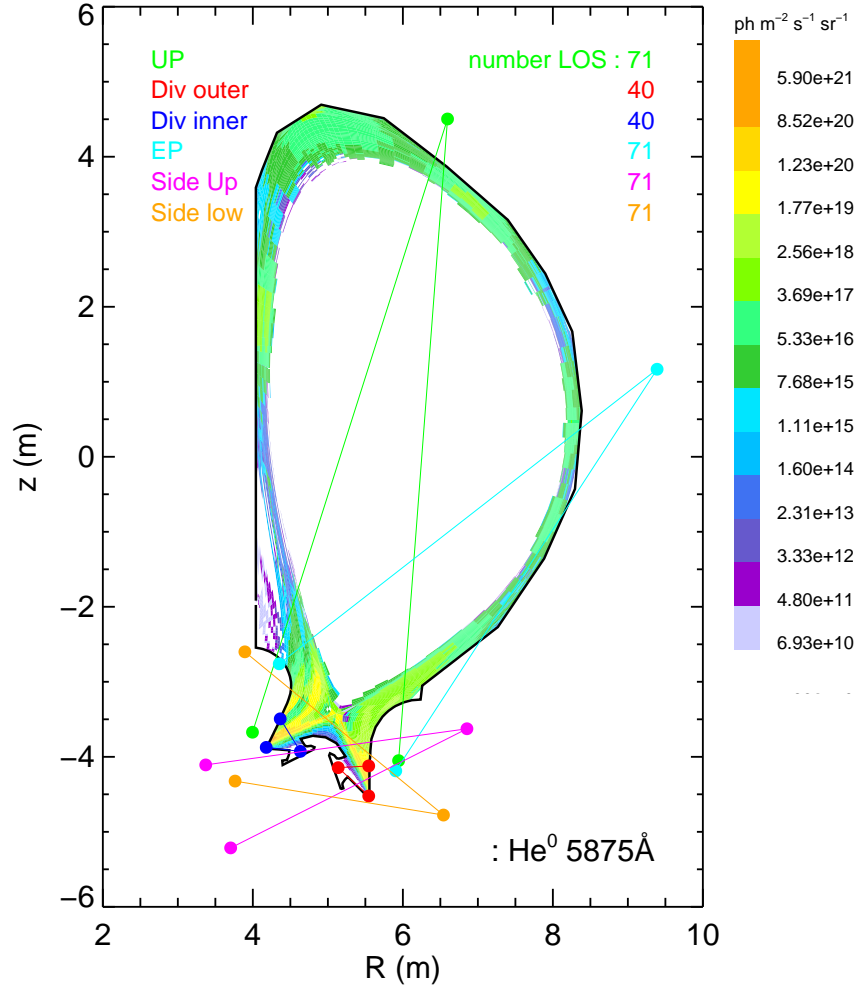


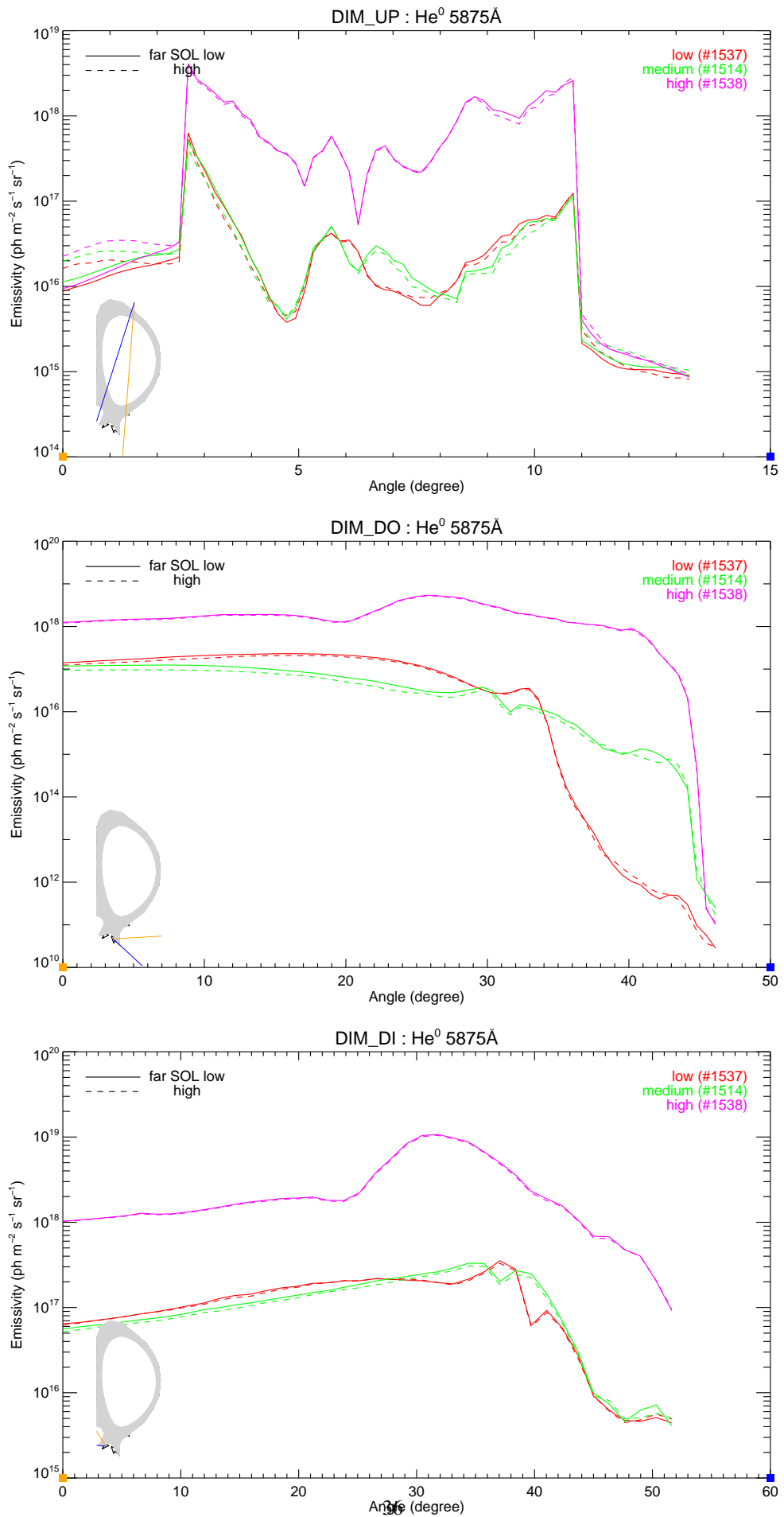


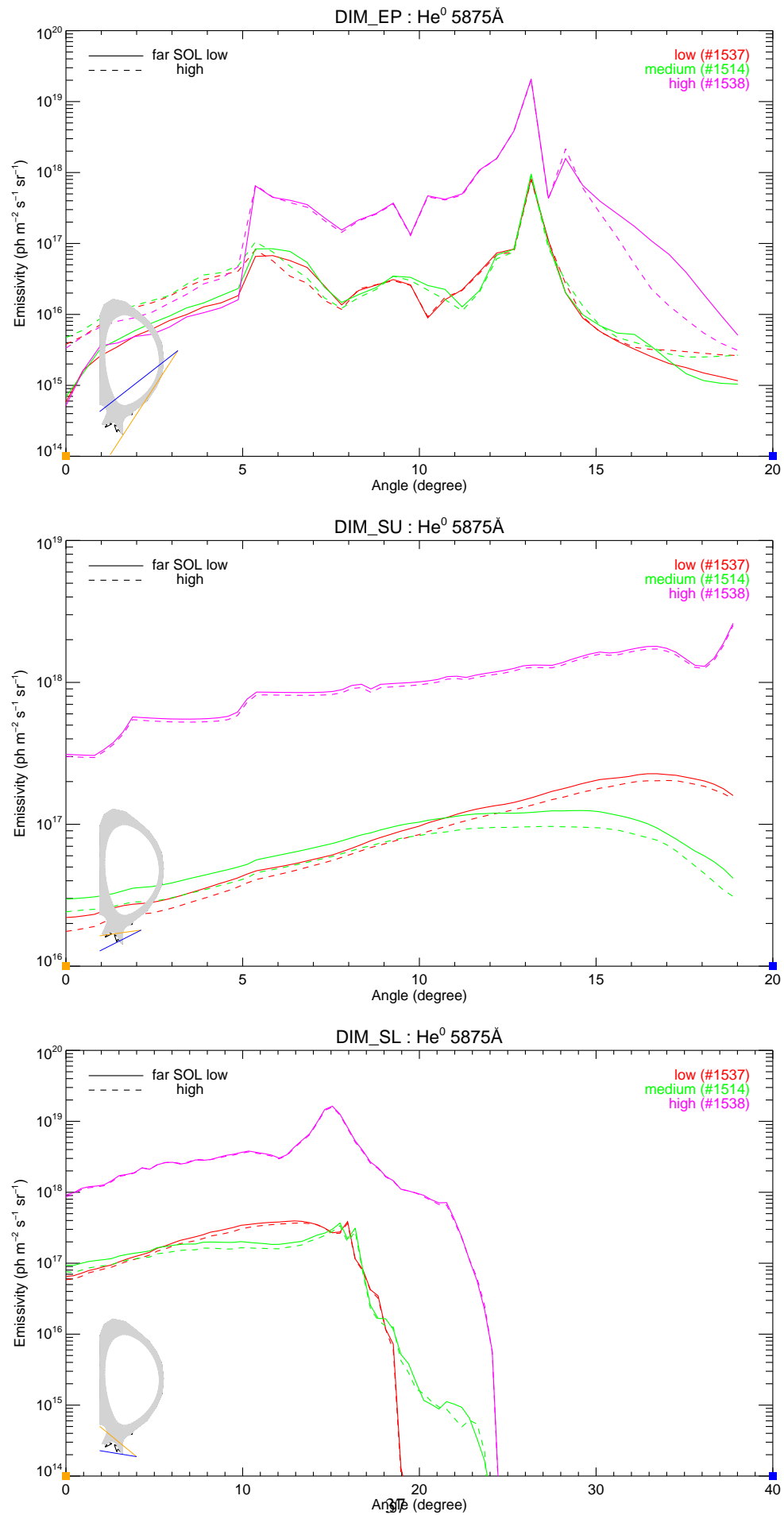
$\text{He}^0 \text{ 5875\AA}$, $1s^2 3d \ ^3D - 1s^2 2p \ ^3P$

Summary of emission (in $10^{18} \text{ ph m}^{-2} \text{ s}^{-1} \text{ sr}^{-1}$) for the peak and minimum values and the LOS intensity at the centre point of the spectrometer fan and the value at the 75th percentile. The figure shows the poloidal distribution for scenario *i-gas-0003-1538-00o*.

Scenario conc. (%)	DIM_UP		DIM_DO		DIM_DI		DIM_EP		DIM_SU		DIM_SL	
	peak min	mid 75th										
i-gas-0003-1537-00d (1.0000)	0.632	0.010	0.230	0.169	0.353	0.218	0.821	0.026	0.227	0.089	0.395	0.269
i-gas-0003-1537-00o (1.0000)	0.570	0.010	0.207	0.156	0.329	0.219	0.793	0.026	0.204	0.078	0.369	0.262
i-gas-0003-1514-00d (1.0000)	0.497	0.030	0.124	0.045	0.332	0.204	0.953	0.033	0.125	0.098	0.369	0.301
i-gas-0003-1514-00o (1.0000)	0.403	0.026	0.096	0.033	0.307	0.184	0.897	0.030	0.097	0.079	0.338	0.281
i-gas-0003-1538-00d (1.0000)	4.098	0.399	5.379	3.200	10.720	3.756	20.761	0.133	2.608	0.988	16.372	16.372
i-gas-0003-1538-00o (1.0000)	0.001	1.133	0.000	2.000	0.092	3.593	0.001	0.447	0.306	1.373	0.000	3.348
i-gas-0003-1538-00o (1.0000)	3.983	0.384	5.204	3.098	10.449	3.652	20.155	0.129	2.522	0.937	15.915	15.915
	0.001	1.005	0.000	1.931	0.097	3.466	0.003	0.452	0.295	1.317	0.000	3.244



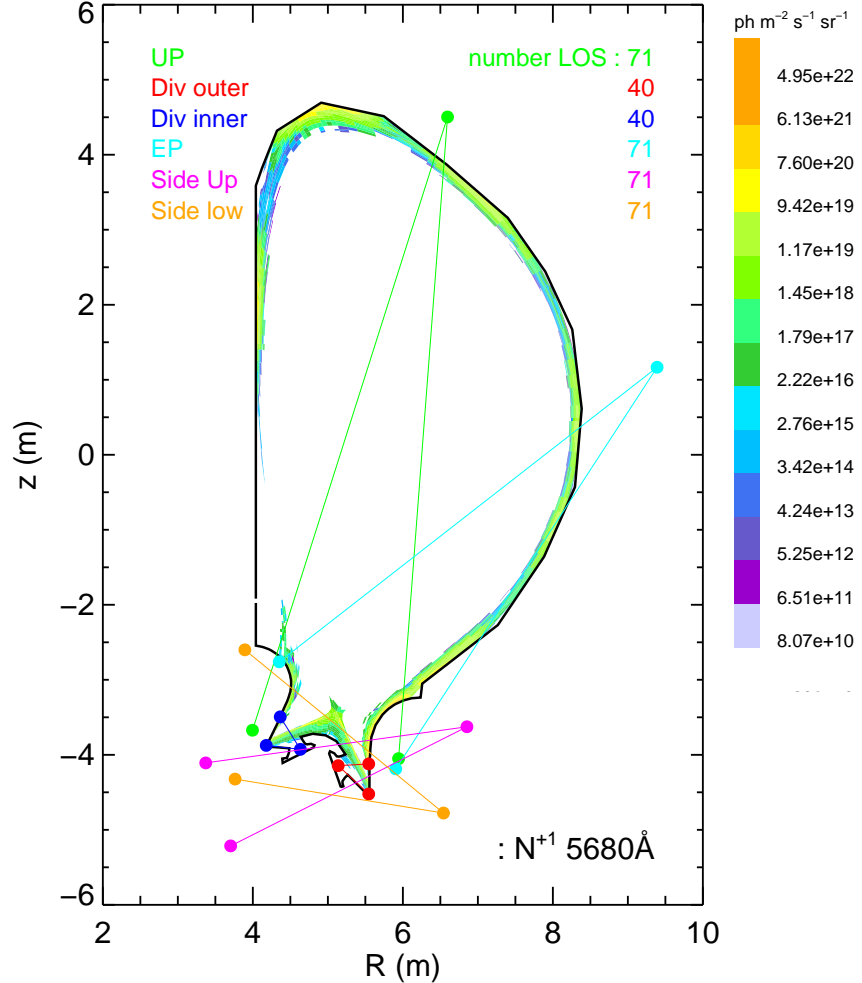


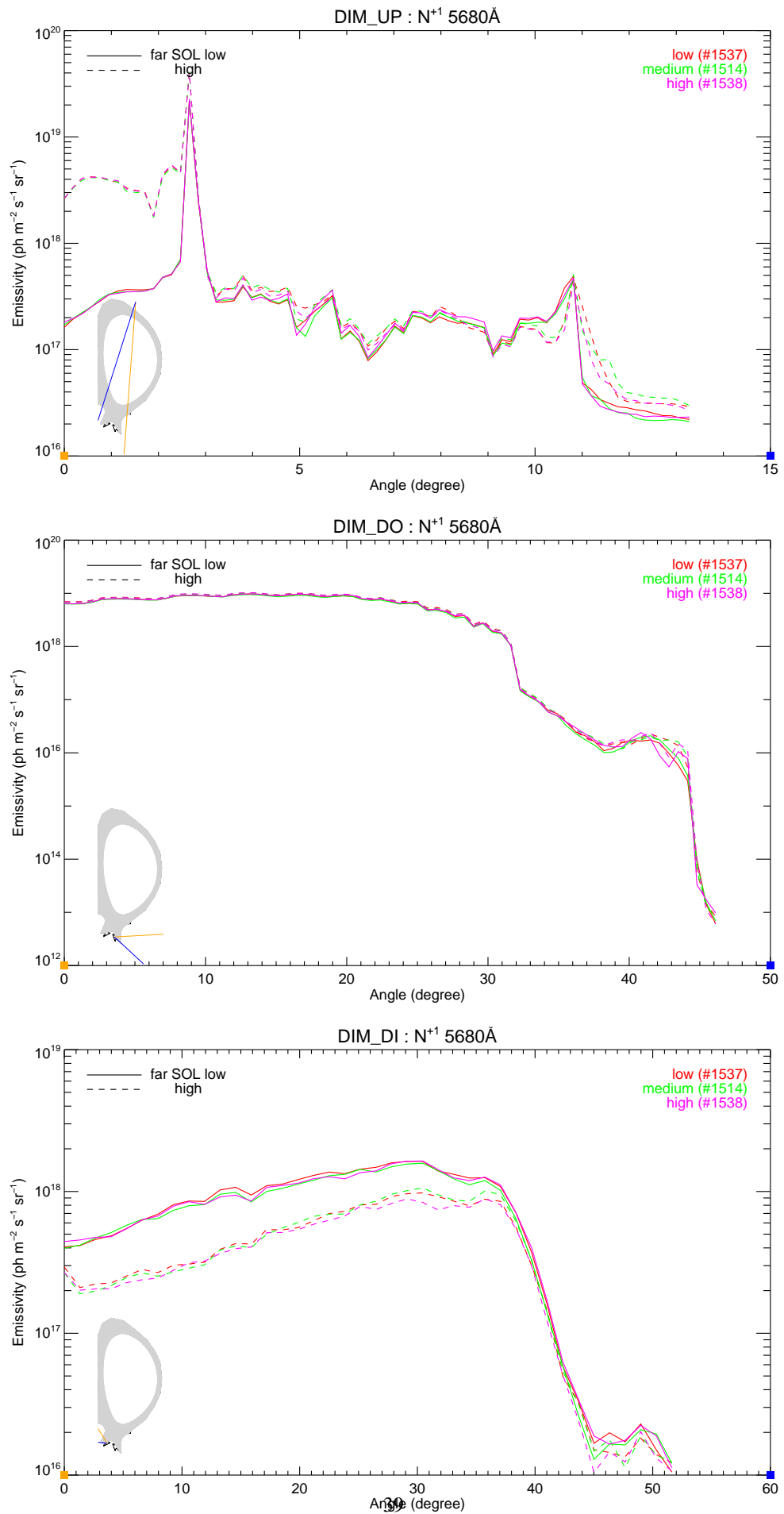


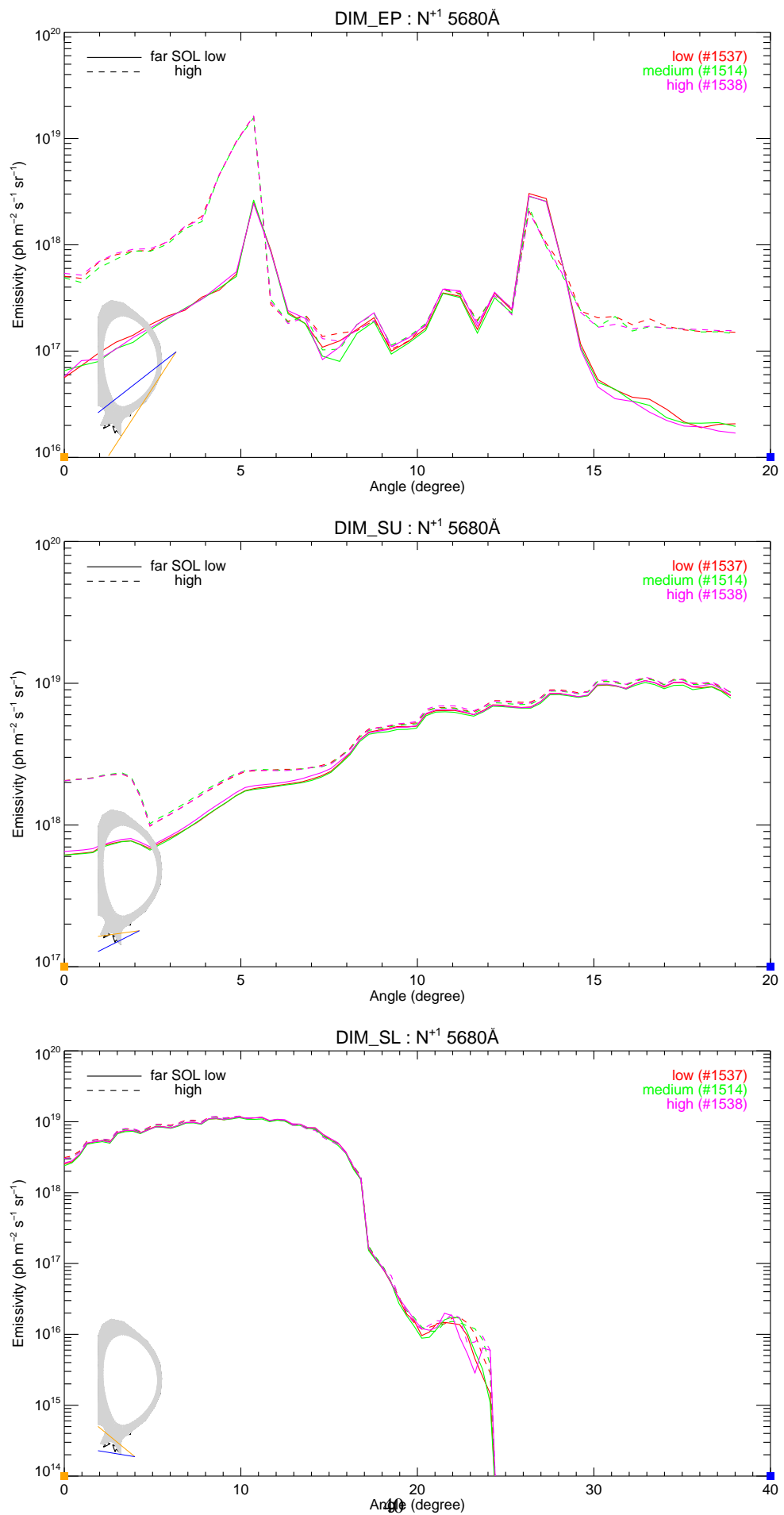
$\mathbf{N^{+1} \text{ 5680\AA}, 2s^2 2p 3p ^3D - 2s^2 2p 3s ^3P}$

Summary of emission (in $10^{18} \text{ ph m}^{-2} \text{ s}^{-1} \text{ sr}^{-1}$) for the peak and minimum values and the LOS intensity at the centre point of the spectrometer fan and the value at the 75th percentile. The figure shows the poloidal distribution for scenario *i-gas-0103-1538-00o*.

Scenario conc. (%)	DIM_UP		DIM_DO		DIM_DI		DIM_EP		DIM_SU		DIM_SL	
	peak min	mid 75th	peak min	mid 75th	peak min	mid 75th	peak min	mid 75th	peak min	mid 75th	peak min	mid 75th
i-gas-0103-1537-00d (1.0000)	21.892 0.022	0.096 0.322	9.755 0.000	7.174 8.748	1.632 0.010	1.480 1.298	3.035 0.019	0.124 0.328	10.455 0.614	4.956 8.258	11.697 0.000	5.713 8.855
i-gas-0103-1537-00o (1.0000)	40.851 0.029	0.124 0.519	10.224 0.000	7.621 9.329	0.977 0.012	0.811 0.793	16.276 1.04	0.124 0.874	10.938 0.982	5.139 8.821	11.941 0.000	5.685 9.198
i-gas-0103-1514-00d (1.0000)	21.779 0.021	0.100 0.306	9.464 0.000	6.893 8.685	1.583 0.012	1.371 1.201	2.850 0.020	0.119 0.317	10.125 0.613	4.715 8.166	11.415 0.000	5.494 8.671
i-gas-0103-1514-00o (1.0000)	40.834 0.030	0.135 0.541	10.119 0.000	7.621 9.256	1.060 0.011	0.854 0.805	15.714 1.03	0.137 0.870	10.838 1.022	5.050 8.672	11.789 0.000	5.508 9.066
i-gas-0103-1538-00d (1.0000)	22.484 0.023	0.106 0.326	9.744 0.000	7.270 8.983	1.642 0.011	1.396 1.230	2.879 0.017	0.133 0.358	10.441 0.650	4.891 8.268	11.714 0.000	5.790 8.919
i-gas-0103-1538-00o (1.0000)	40.356 0.027	0.115 0.500	10.327 0.000	7.504 9.379	0.888 0.010	0.746 0.740	16.366 0.109	0.135 0.908	11.059 0.989	5.174 8.728	12.023 0.000	5.276 9.106



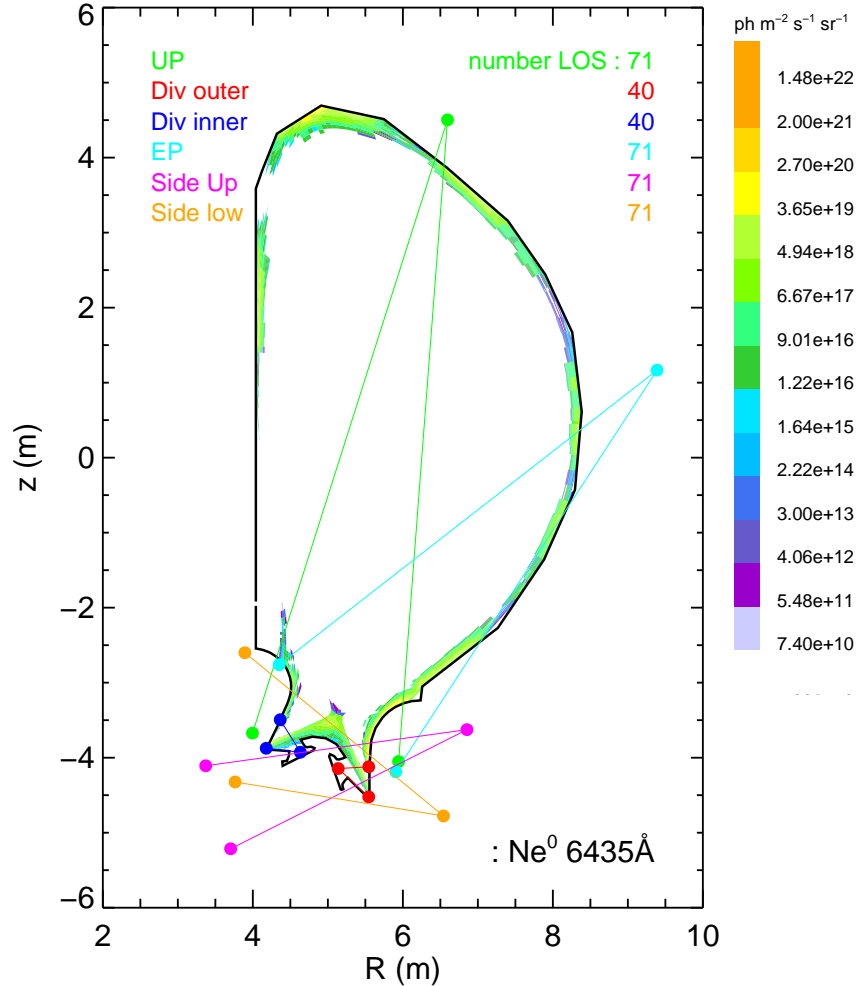


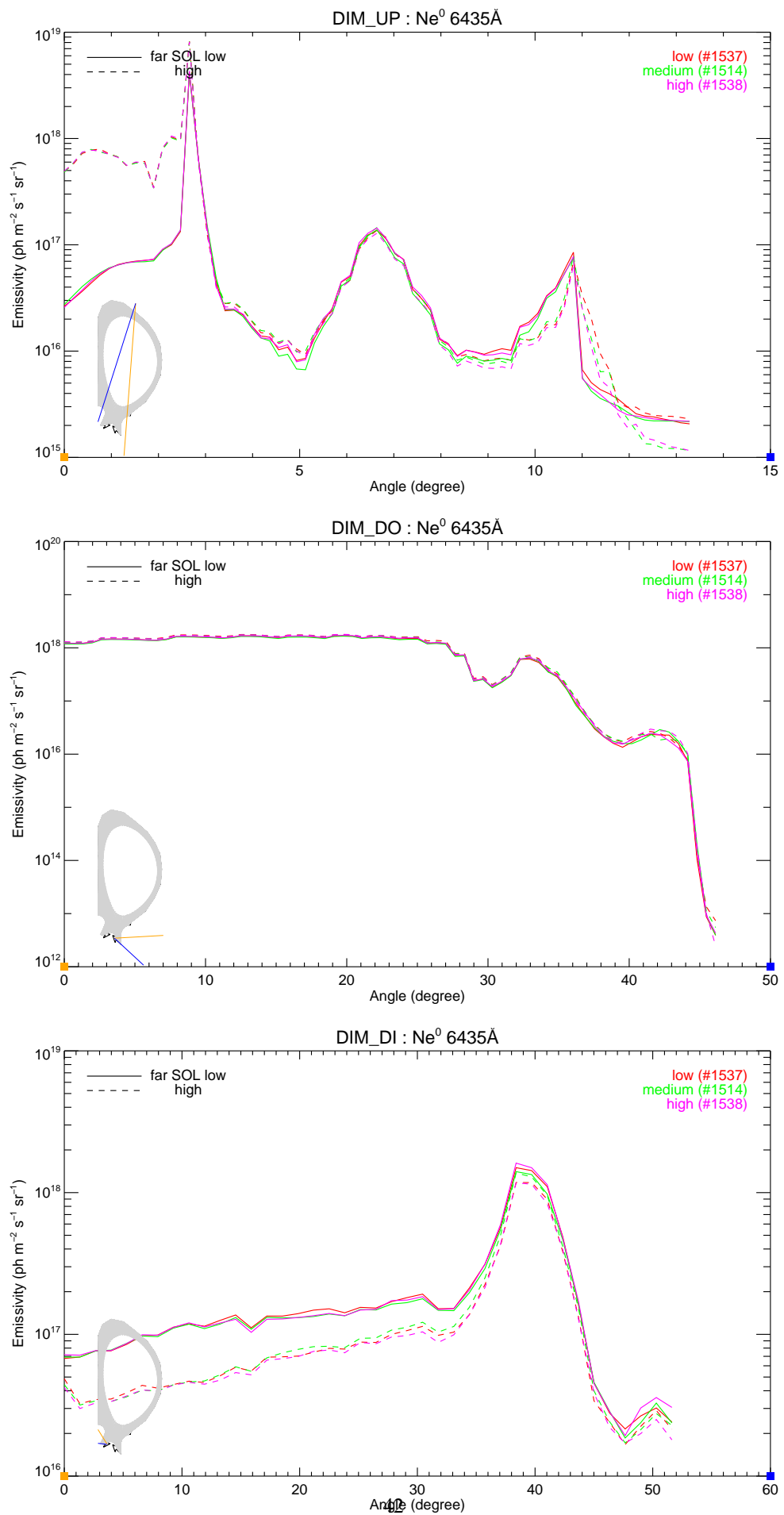


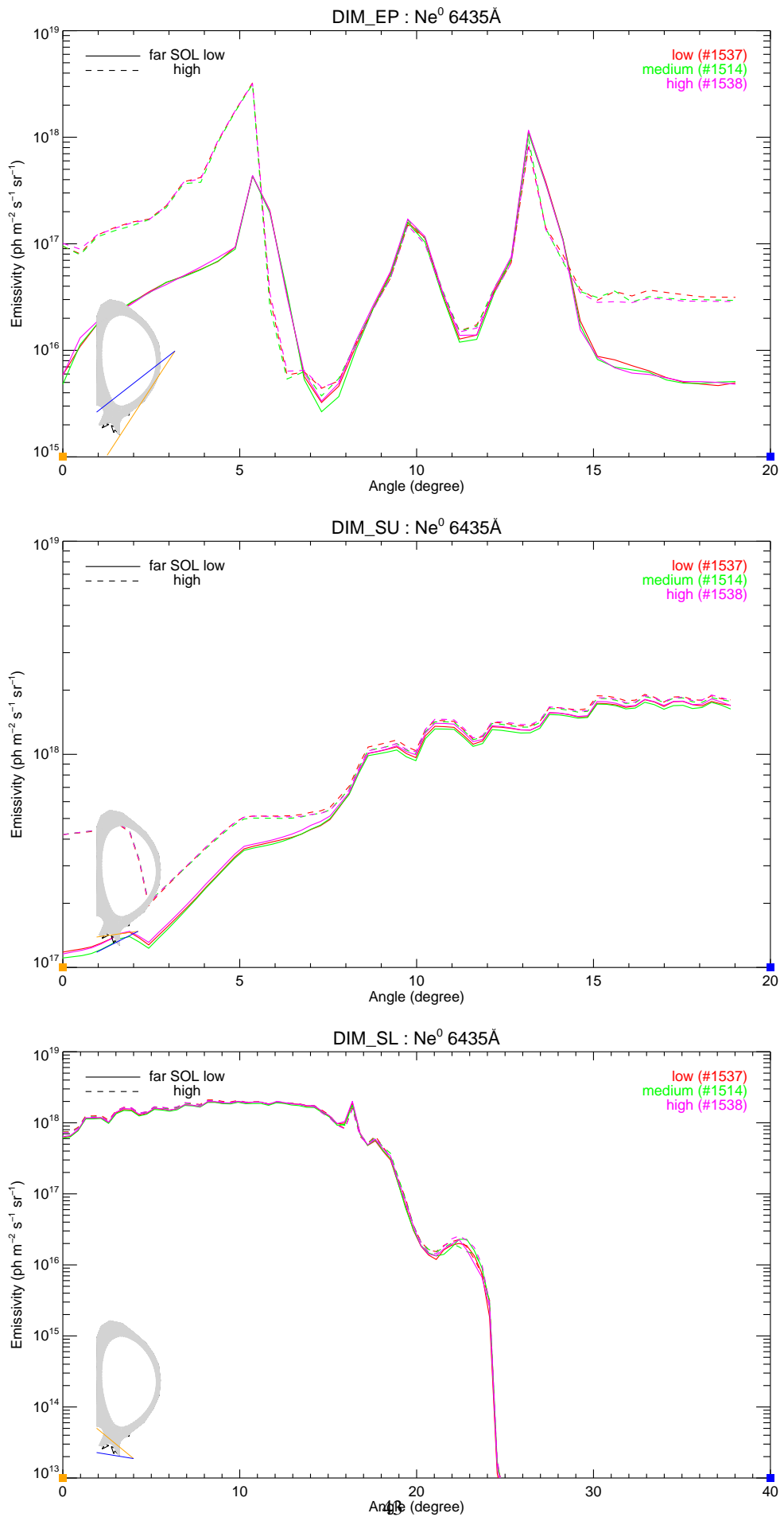
$\text{Ne}^1 \text{ 6435\AA}, 2\text{p}^5(^2\text{P}_{1/2}) 3\text{s}0.5 - 2\text{p}^5(^2\text{P}_{3/2}) 3\text{s}1.5$

Summary of emission (in $10^{17} \text{ ph m}^{-2} \text{ s}^{-1} \text{ sr}^{-1}$) for the peak and minimum values and the LOS intensity at the centre point of the spectrometer fan and the value at the 75th percentile. The figure shows the poloidal distribution for scenario *i-gas-0103-1538-00o*.

Scenario conc. (%)	DIM_UP		DIM_DO		DIM_DI		DIM_EP		DIM_SU		DIM_SL	
	peak min	mid 75th	peak min	mid 75th	peak min	mid 75th	peak min	mid 75th	peak min	mid 75th	peak min	mid 75th
i-gas-0103-1537-00d (1.0000)	41.767 0.021	1.370 0.681	16.819 0.000	15.471 0.215	14.994 1.702	1.533 0.032	11.349 0.682	1.592 1.180	18.047 15.603	10.843 0.000	19.975 17.148	12.331
i-gas-0103-1537-00o (1.0000)	82.139 0.023	1.370 1.370	17.832 0.000	16.473 16.889	11.778 0.167	0.876 1.063	32.362 0.044	1.505 1.505	19.108 1.951	11.674 16.544	21.022 0.000	12.820
i-gas-0103-1514-00d (1.0000)	41.331 0.022	1.382 0.658	16.578 0.000	14.860 15.483	14.059 0.186	1.486 1.650	10.909 0.027	1.577 0.689	17.552 1.108	10.483 15.315	19.472 0.000	12.055
i-gas-0103-1514-00o (1.0000)	81.210 0.012	1.452 1.452	17.460 0.000	16.250 16.628	13.750 0.172	0.943 1.137	31.472 0.037	1.668 1.476	18.686 2.001	11.233 16.342	20.406 0.000	12.302
i-gas-0103-1538-00d (1.0000)	42.995 0.022	1.437 0.677	17.219 0.000	15.535 16.051	16.147 0.193	1.502 1.728	11.654 0.033	1.704 0.744	18.200 1.157	10.981 15.621	20.142 0.000	12.565
i-gas-0103-1538-00o (1.0000)	80.898 0.012	1.286 1.286	17.951 0.000	16.410 16.796	11.740 0.171	0.858 0.993	31.914 0.045	1.491 1.491	18.992 1.984	11.234 16.569	20.512 0.000	11.757



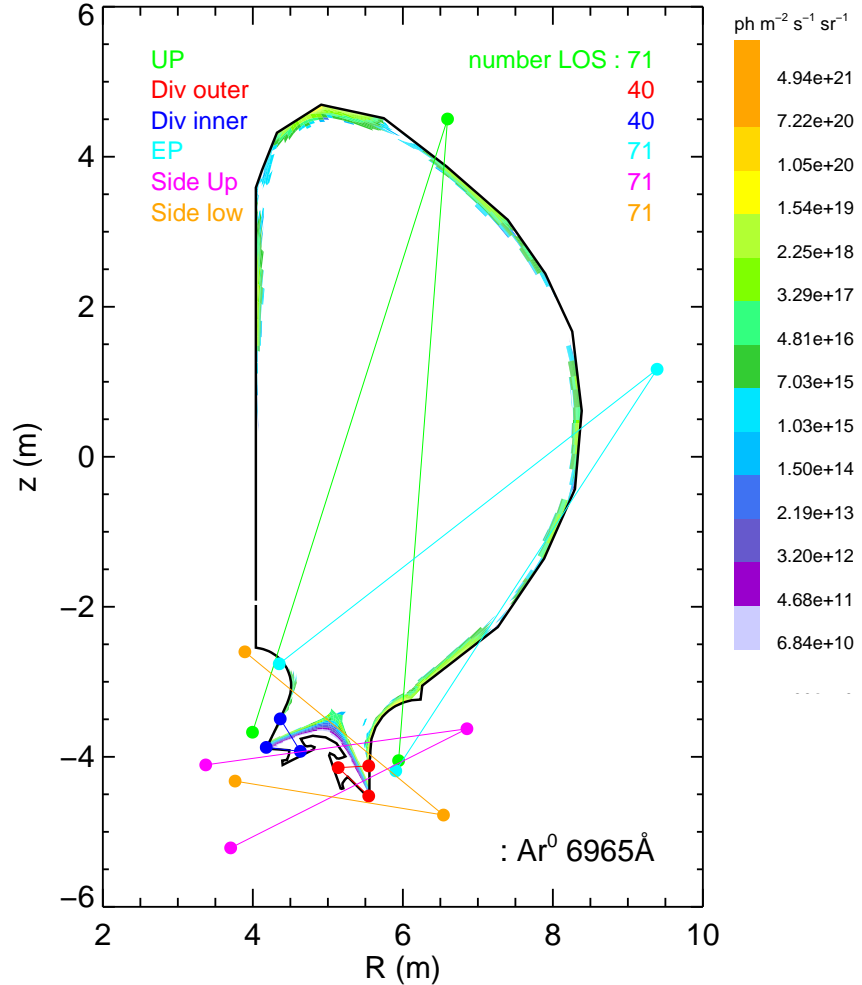


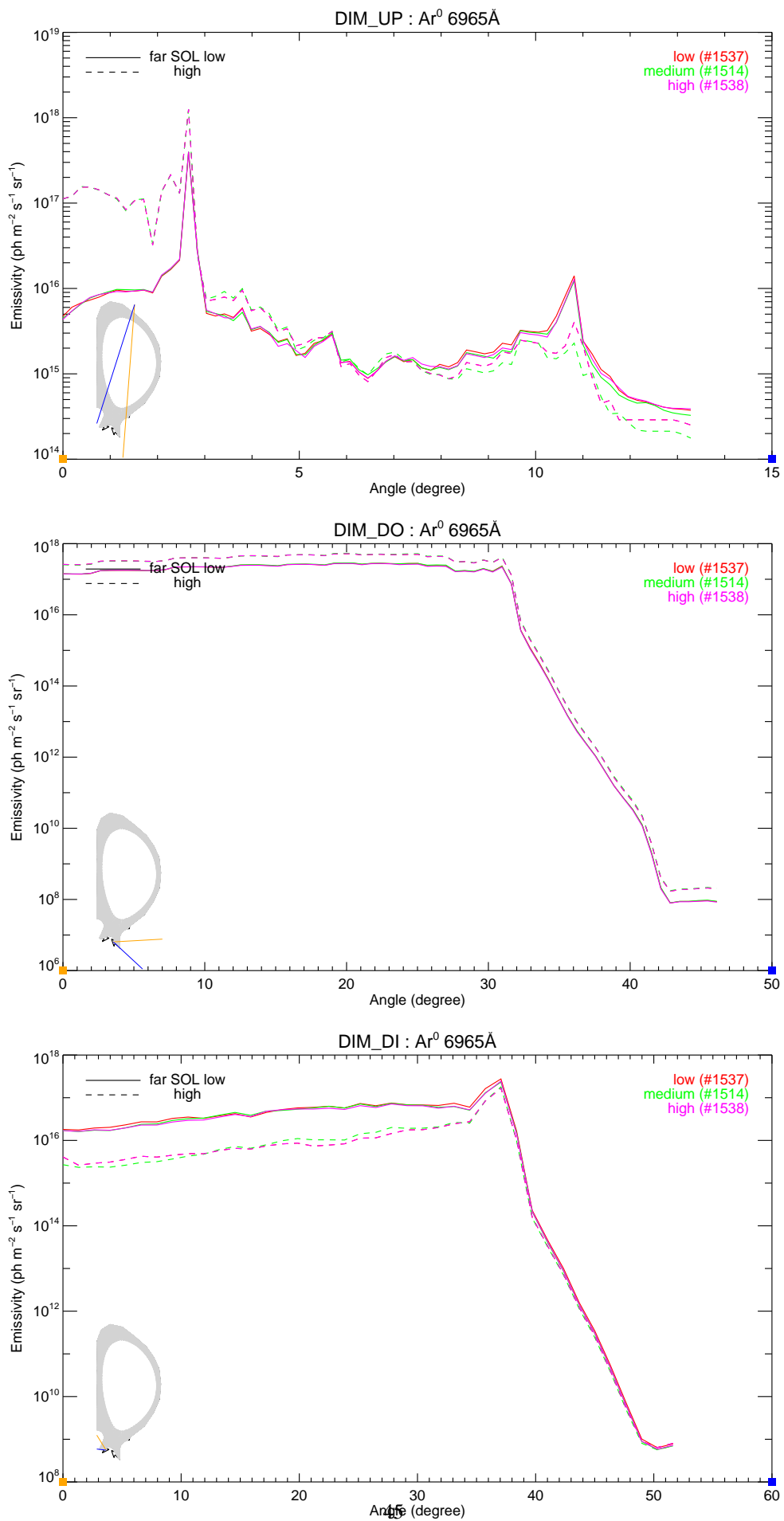


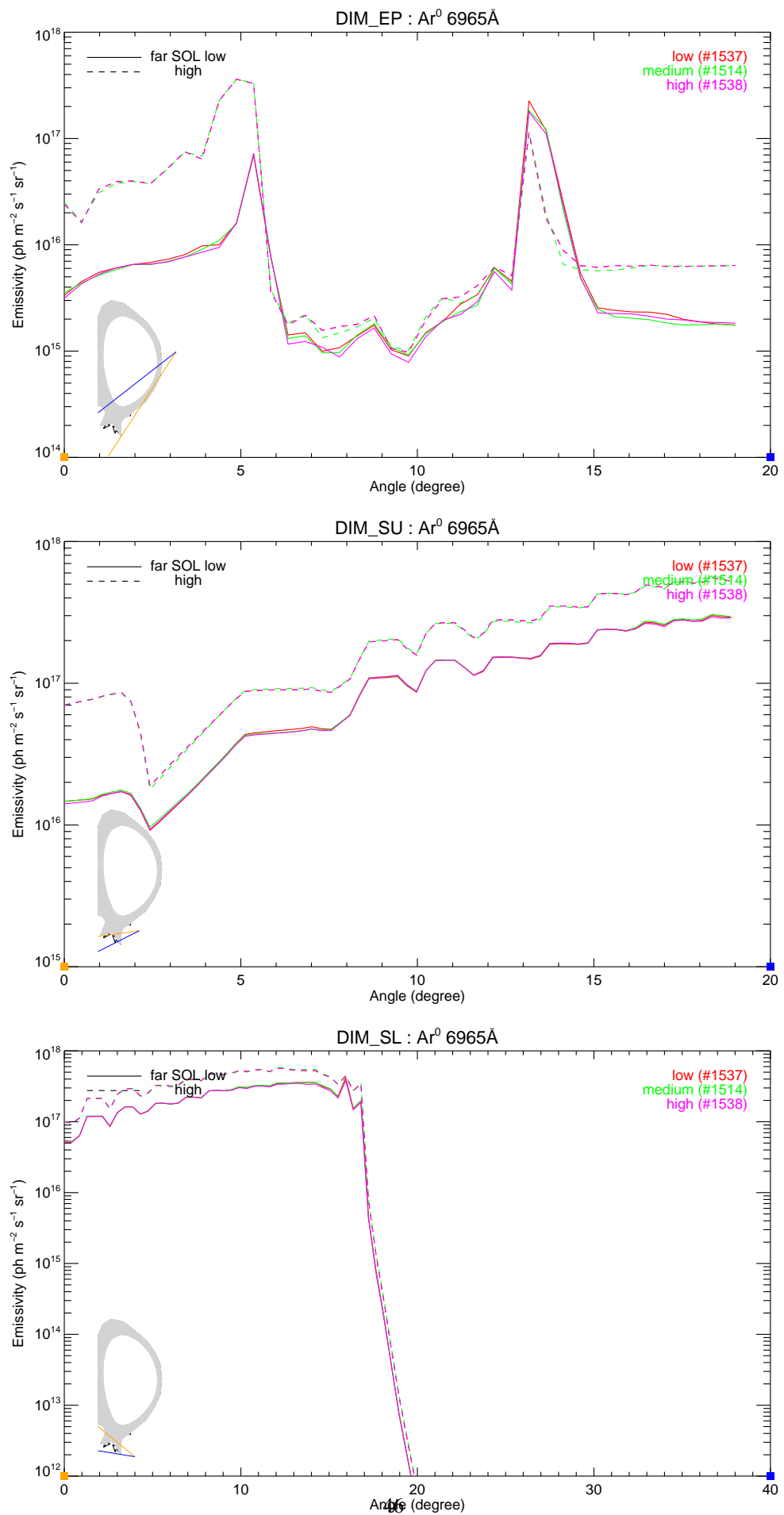
$\text{Ar}^0 \text{ 6965\AA}$, $3p^5 4p \ ^3P_1 - 3p^5 4s \ ^3P_2$

Summary of emission (in $10^{17} \text{ ph m}^{-2} \text{ s}^{-1} \text{ sr}^{-1}$) for the peak and minimum values and the LOS intensity at the centre point of the spectrometer fan and the value at the 75th percentile. The figure shows the poloidal distribution for scenario *i-gas-0303-1538-00o*.

Scenario conc. (%)	DIM_UP		DIM_DO		DIM_DI		DIM_EP		DIM_SU		DIM_SL	
	peak min	mid 75th	peak min	mid 75th	peak min	mid 75th	peak min	mid 75th	peak min	mid 75th	peak min	mid 75th
i-gas-0303-1537-00d (1.0000)	3.940 0.004	0.011 0.060	2.836 0.000	2.749 2.493	2.753 0.000	0.649 0.631	2.263 0.009	0.009 0.073	3.007 0.092	1.115 1.901	4.198 0.000	2.874 2.735
i-gas-0303-1537-00o (1.0000)	12.475 0.003	0.011 0.095	5.218 0.000	4.898 4.590	1.668 0.000	0.115 0.113	3.613 0.010	0.010 0.375	5.538 0.189	2.032 3.502	5.672 0.000	4.234 4.404
i-gas-0303-1514-00d (1.0000)	3.981 0.003	0.011 0.054	2.879 0.000	2.747 2.540	2.324 0.000	0.623 0.597	1.831 0.009	0.009 0.070	3.062 0.097	1.132 1.926	3.883 0.000	2.914 2.741
i-gas-0303-1514-00o (1.0000)	12.528 0.002	0.013 0.100	5.369 0.000	4.994 4.518	1.785 0.000	0.155 0.143	3.595 0.010	0.010 0.376	5.696 0.179	2.072 3.462	5.847 0.000	4.313 4.530
i-gas-0303-1538-00d (1.0000)	3.972 0.004	0.011 0.058	2.773 0.000	2.714 2.456	2.440 0.000	0.590 0.568	1.774 0.008	0.008 0.069	2.940 0.093	1.139 1.919	3.840 0.000	2.735 2.735
i-gas-0303-1538-00o (1.0000)	12.475 0.003	0.011 0.095	5.218 0.000	4.898 4.590	1.668 0.000	0.115 0.113	3.613 0.010	0.010 0.375	5.538 0.189	2.032 3.502	5.672 0.000	4.234 4.404







Chapter 5

Working visits to ITER

Fifty working days per year are assigned to ITER on atomic physics and diagnostic design. Support calculations and presentations for two conceptual design reviews, on bolometer and core X-ray spectroscopy, were undertaken in 2012 and 2013.

Date		
31-01-12	–	03-02-2012
06-02-12	–	10-02-2012
20-01-12	–	23-02-2012
14-03-12	–	16-03-2012
19-03-12	–	20-03-2012
30-05-12	–	01-06-2012
05-07-12	–	06-07-2012
09-07-12	–	13-07-2012
26-08-12	–	27-08-2012
10-09-12	–	11-09-2012*
05-12-12	–	09-12-2012

Table 5.1: Summary of dates of working visits to ITER in 2012. * Location: NFRI in Daejeon, Korea.

Date		
04-02-13	–	08-03-2013
11-02-13	–	15-03-2013
25-02-13	–	01-03-2013
08-04-13	–	12-04-2013
06-05-13	–	10-05-2013
03-06-13	–	07-06-2013
24-06-13	–	28-06-2013
01-07-13	–	05-07-2013
08-07-13	–	12-07-2013
26-08-13	–	30-08-2013
09-09-13	–	13-09-2013
16-09-13	–	20-09-2013
14-10-13	–	18-10-2013
21-10-13	–	25-10-2013
02-12-13	–	06-12-2013
09-12-13	–	13-12-2013

Table 5.2: Summary of dates of working visits to ITER.

Bibliography

- [1] R. Barnsley, M. O'Mullane, L. C. Ingesson and A. Malaquias. ‘Design study for International Thermonuclear Experimental Reactor high resolution x-ray spectroscopy array’. Rev. Sci. Instrum., **75** (2004) 3743–3746. [doi:10.1063/1.1790044](https://doi.org/10.1063/1.1790044)
- [2] H. Meister, M. Willmeroth, D. Zhang, A. Gottwald, M. Krumrey and F. Scholze. ‘Broad-band efficiency calibration of ITER bolometer prototypes using Pt absorbers on SiN membranes’. Europhysics Conference Abstracts (Proc. of the 40th EPS Conference on Plasma Physics, Espoo, Finland, 2013) , (European Physical Society, Geneva), **37D** (2013) P5.106. Available from: <http://ocs.ciemat.es/EPS2013PAP/pdf/P5.106.pdf>
- [3] J. Wesson. ‘Poloidal distribution of impurities in a rotating tokamak plasma’. Nucl. Fusion, **37**(5) (1997) 577–581. [doi:10.1088/0029-5515/37/5/I01](https://doi.org/10.1088/0029-5515/37/5/I01)
- [4] T. Sugie, H. Ogawa, A. Katsunuma, M. Maruo, Y. Kita, K. Ebisawa and T. A. S. Kasai. ‘Design of Divertor Impurity Monitoring System for ITER (II)’. JAERI-Tech 98-047, JAERI, Japan (1998). Available from: <http://jolissrch-inter.tokai-sc.jaea.go.jp/pdfdata/JAERI-Tech-98-047.pdf>
- [5] H. Ogawa, T. Sugie, A. Katsunuma and S. Kasai. ‘Design of Impurity Influx Monitor (Divertor) for ITER’. JAEA-Technology 2006-015, JAEA, Japan (2002). Available from: <http://jolissrch-inter.tokai-sc.jaea.go.jp/pdfdata/JAEA-Technology-2006-015.pdf>
- [6] A. Iwamae, T. Sugie, H. Ogawa and Y. Kusama. ‘Synthesized intensity of emission lines of hydrogen isotopes and impurities in the ITER divertor plasma’. Plasma Phys. Control. Fusion, **53**(4) (2011) 045005. [doi:10.1088/0741-3335/53/4/045005](https://doi.org/10.1088/0741-3335/53/4/045005)
- [7] D. P. Coster. SOLPS Manual. Available from: <http://solps-mdsplus.aug.ipp.mpg.de:8080/solps/Documentation/solps.pdf>
- [8] D. Reiter. ‘The Eirene Code User Manual, Version 11/2009’. Technical report, Institut fuer Energie- und Klimaforschung, Plasmaphysik (IEK-4), Forschungszentrum Juelich (2009)
- [9] A. S. Kukushkin, H. D. Pacher, V. Kotov, G. W. Pacher and D. Reiter. ‘Finalizing the ITER divertor design: The key role of SOLPS modeling’. Fusion Eng. Design., **86**(12) (2011) 2865–2873. ISSN 0920-3796. [doi:10.1016/j.fusengdes.2011.06.009](https://doi.org/10.1016/j.fusengdes.2011.06.009)
- [10] H. P. Summers (2007). Atomic Data and Analysis Structure User Manual. Available from: <http://www.adas.ac.uk>